JOINT EUROPEAN TORUS

JET–P(90)49

M. Bures, J. Jacquinot, K. Lawson, M. Stamp, H.P. Summers,
D.A. D'Ippolito and JET Team

Impurity Release from the ICRF Antenna Screens in JET

Impurity Release from the ICRF Antenna Screens in JET

M. Bures, J. Jacquinot, K. Lawson, M. Stamp, H.P. Summers,
D.A. D'Ippolito[1] and JET Team*

JET-Joint Undertaking, Culham Science Centre, OX14 3DB, Abingdon, UK

[1]Lodestar Research Corporation, Boulder, Colorado, USA
** See Appendix 1*

Preprint of Paper to be submitted for publication in
Plasma Physics and Controlled Fusion

ABSTRACT.

During the ICRF(Ion Cyclotron Range of Frequencies) heating on JET(Joint European Torus) the highly localised impurity influxes from the Faraday screens(FS) of RF antennas are observed. The influxes result from the acceleration of deuterium and impurity ions in the RF enhanced Bohm-Debye sheaths. The RF enhanced sheaths form when a magnetic field line, linking a large RF magnetic flux, connects two surfaces and closes a loop where the RF voltage is induced. The FS influxes depend on two intimately linked parameters, antenna voltage and the density at FS, as well as on the magnetic field angle, antenna phasing, FS geometry and material. The influx of Beryllium(Be) from the front face of the Be–gettered FS is $\phi_{Be}^{FS} = 3 = 1x10^{19}$ atoms MW^{-1} s^{-1}in monopole($k_{||} = 0m^{-1}$) phasing when the torus had carbon(C) belt limiters. The contribution of the Be front face influx and the remaining Ni influx from the FS gaps to the ion dilution is $\delta Z_{eff}/P_{RF} < 0.015$ MW^{-1}. When the C-belt limiters were replaced by the Be-belt limiters, the influxes were reduced by more than a factor of 2. In the dipole phasing($k_{||} = 7m^{-1}$) the front fac influx is negligible.

1.0 Introduction.

ICRF heating of the tokamaks has been successfully used on a number of devices[JACQUINOT 1988, ODAJIMA 1986, STEINMETZ 1989, WEYNANTS 1988, WILSON 1988]. A major drawback of the ICRF heating was the gas and impurity release associated with the RF pulse. In JET, as elsewhere, a density rise and an increase in radiated power were observed. Depending on the amount of the deuterium desorption, Z_{eff} remained either constant or increased, the latter implying an enhanced ion dilution. The density limit achieved with the RF heating was only marginally higher than in the ohmic phase of the discharge. Successful coupling of large amounts of RF power into an H–mode was not possible.

Recently, the RF impurity situation in JET was radically improved. It can be accounted for by a number of factors. The most important were the introduction of Beryllium(Be) as a wall(Be–gettering) and limiter material(Be–belt limiters). Equally important is the coverage of the nickel(Ni) antenna screens by a Be layer, which together with the dipole phasing(k_{II}=7 m^{-1}) and the high RF wave absorption per pass allowed for a very successful operation of the ICRF heating system. The previously observed RF density limit was exceeded by more than a factor of two. A high quality H–mode was obtained with RF heating alone[JACQUINOT 1990] and combined with NBI(neutral beam injection).

On JET, the RF induced influxes can be categorized into three groups. First, the most important one[BUREŠ 1990b,c], is the "global" impurity influx(not specific to the heating method) associated with the RF power conducted into the scrape–off layer(SOL) from the bulk of the plasma, $P_{II}=P_{\Omega}+P_{RF}-P_{RAD}$. During the RF pulse the parallel energy flow in the SOL increases and the sputtering in the Bohm–Debye sheaths at the limiter and wall surfaces rises as a function of the electron temperature. The characteristic time associated with the released influxes is comparable to the incremental confinement time of the RF energy $\tau^{E}_{INC} \approx \delta W/(P_{RF}-\delta P_{\Omega})$, where δW is the increase of the plasma stored energy and δP_{Ω} is the usually observed drop in the ohmic power. This process is a general mechanism

which will arise whenever any power, not necessarily RF, is applied to heat the plasma. It should be resolved in a more general context and the recent proposal for JET extension[THOMAS 1990] adresses this particular issue.

The second type of influx identified on JET[BUREŠ 1988b, 1990b,c] is a fast influx from the limiters and wall which was observed before conditioning techniques, such as carbonisation, helium discharge cleaning and Be gettering were systematically employed. The characteristic time associated with these influxes was typically $\tau \simeq 10$ ms or less, indicating that an RF field interaction with the vessel surfaces was taking place rather than the increase of the power flow in the SOL. Indeed, with the tokamak properly conditioned, these influxes are not observed anymore. The fact that a prompt source of impurities and neutral gas influx is not seen, neither at the limiter nor at the wall, is indirect evidence that no significant fraction of the RF power is directly coupled into the edge of the plasma.

The third, and only remaining "RF specific" influx clearly identified on JET[BEHRINGER 1986a, BUREŠ 1988a,1990b], is the influx from the Faraday screen(FS) of the RF antennae. It results from the interaction of the large amplitude oscillating field and the plasma close to the surface of FS. The experimental observations and the influx scaling are consistent with ion sputtering in the RF enhanced sheaths which form at the front face of the FS and also in the gaps between the FS elements[PERKINS 1989, MYRA 1990, D'IPPOLITO 1990a]. In general, RF sheaths will form at the points of contact between the magnetic field lines, linking a large RF magnetic flux, and the material surfaces. The time scale of these influxes is very short, $\tau < 10$ ms.

One important aspect of the JET results should be pointed out here. JET is a large device with plasma parameters close to the reactor range. This implies a high RF wave absorption per pass. The resulting RF field pattern is highly localised around the antennae. This enables the separation of the "global" influxes from the "RF specific" ones by localised measurements at the antennae screens, limiters and the wall. In smaller devices a similar distinction and, in particular, a quantitative estimate of the different contributions

is not easy to make.

In this paper we will summarise the observations of the FS influxes from the different JET antennae, give their scaling with the plasma and antenna parameters, estimate the contribution of these influxes to Z_{eff}, and compare the observations with the predictions of a theoretical model. The theoretical model itself, and some preliminary comparisons with JET results, are presented in a separate publication[D'Ippolito 1990b]. The two papers taken together present compelling evidence that the physical origin of the FS influxes is understood. Finally, the substantial reduction of the FS influxes, to very low levels, by the implementation of various design and operational elements will be pointed out.

2.0 Experimental arrangements.

The JET device is a low aspect ratio tokamak with the major radius R=3 m and the minor radius a=1.2 m. The elongation is typically κ=1.4–1.6 and the maximum magnetic field on axis is B_0=3.4 T. The plasma current, in the discharges discussed in this paper, did not exceed I_p=3 MA. The RF heating system consisted originally (period 1985–1986) of three A_0 antennae of prototype design[KAYE 1985]. Each was able of delivering 3 MW of RF power in the frequency range 23 – 57 MHz. The characteristic feature of the A_0 antennae, relevant to the subject discussed in this paper, is that the front face of the FS was flat. Before installation in the vessel, one of the antennae was coated by a 1μm chromium(Cr) layer. Schematic cross sections of the A_0 and A_1 antennae are shown in Fig.1. The FS of both antennae were made of Ni. The important feature of the A_1 screen[KAYE 1987] is the V–shaped indentation which was implemented to avoid direct interaction of the plasma with the FS due to ripple of the magnetic field. The characteristic distance δs between the Antenna Tile Tangency Surface(ATTS) and the FS is different in the two cases. In the case of the A_0 antenna it is typically 4–5 mm while in the case of the A_1 antenna it is in the range 8–10 mm. The parallel connection length relating to the "private SOL" of both antennas is very similar, $L_{II}^1 \approx$ 0.2 m. Eight A_1 antennae were

operated on JET during the period 1987–1989 with a power capability 3 to 4 MW per antenna depending on the level of the generator upgrade. Both A_0 and A_1 antennae had the capability of exciting a k_{II} spectrum which peaked either at k_{II}=0 m^{-1} (called monopole) or at k_{II}=7 m^{-1}(since 1987 called toroidal dipole). The most widely used heating scenarios were D(H),^{4}He(H) and D(^{3}He), with minority species indicated in the brackets. The frequency was usually adjusted so as to place the minority resonace layer on axis. In the experiments described below, hydrogen was used as the resonating species. Four different experimental situations are discussed in this paper. First is the operation of three A_0 antennae in a non–conditioned JET with eight discrete C limiters. One FS was coated with Cr. The second case is the operation of eight A_1 antennae with the Ni FS when the JET device was fitted with two C–belt limiters. The last two cases refer to the Be–gettering phase, one with the C–belt limiters and the other with the Be–belt limiters. The typical thickness of the deposited Be layer on the FS was ≈ 300 Å.

3.0 Overwiew of experimental results.

3.1 Summary of the Faraday screen influx behaviour.

The most important experimental aspects of the FS influxes can be summarised according to their dependence on the plasma and the antenna parameters. It was found that FS influxes depend on, or are characterised by:

1) localisation to the powered antenna

2) angle between the magnetic field at the plasma edge and the FS elements

3) antenna voltage(power at constant coupling resistance)

4) antenna phasing(k_{II} spectrum), FS geometry

5) FS material

6) plasma edge density

7) general level of impurities.

These dependences are consistent with the FS sputtering by deuterium and impurity ions,

including self–sputtering by ions from the FS material, accelerated in the RF and Debye sheaths as proposed in [PERKINS 1989, D'IPPOLITO 1990a and MYRA 1990]. It will be shown below that the original models have to be extended to include the sputtering of the front face of the FS. We proceed with an expanded discussion of each of these observed dependences.

3.2 Localisation of FS influxes to the powered antenna.

To establish the dependence of FS influxes on power, a direct measure of the FS influx is highly desirable. For a Ni FS, this proved to be difficult. No suitable low ionisation state line of the Ni exists which could be monitored by the existing telescopic system capable of viewing some of the antennae. However, the experiment with the Cr coated A_0 antenna FS provided the possibility of monitoring the intensity of the CrI(4254.35 Å) line, which can be related to the neutral Cr influx[Behringer 1989]. As shown in Fig.2, a Cr influx is observed only when the antenna is powered. Note that the power emitted by the adjacent antenna does not release any Cr at all. These conclusions were previously drawn[BEHRINGER 1986, BUREŠ 1988a] from the VUV measurements of the high ionisation stages of Ni and Cr, e.g., CrXXI(149.89 Å), CrXXII(223.01Å), NiXXV(117.94 Å) and NiXXVI(165.35 Å). The characteristic time of the CrI response to the RF power is τ<10 ms. It is clear that the Cr influx cannot be correlated to the parallel power flow in the main SOL in front of the antenna. It is a result of the interaction of the RF oscillating field with the plasma close to the surface of the FS. The localisation of this interaction is consistent with the RF field being highly localised around the antenna and decaying rapidly both in the toroidal and poloidal directions. Such field patterns are excited in JET because of the high single pass absorption efficiency, which is in the range 50–90%.

3.3 FS influx dependence on FS angle with respect to B_{edge}.

The FS elements of JET antennae were installed at an angle of 15^{o} with respect to the

toroidal direction. This implies that the elements are aligned with the total magnetic field at the edge during 5 MA discharges at the full toroidal field B_T=3.4 T. In most of the discharges the typical angle is ≈ 5–10^o. Experiments in which direction of the toroidal field was reversed (where the angle FS–B_T was ≈ 25^o) were discussed in previous publications[JACQUINOT 1988, BUREŠ 1990]. The FS influxes of Ni, were enhanced in these cases by more than a factor 2–4. These experiments were performed with the A_1 antennae(Ni screens) and the C–belt limiters.

3.4 FS influx dependence on antenna voltage.

It was apparent already during early operation that the level of Ni contamination in the plasma scaled with RF power[DENNE 1985]. The VUV spectral line intensities of the high ionisation stages of Ni, INiXXV and INiXXVI, normalised to the plasma density was used as a measure of the Ni content in the plasma. INiXXV/$<n_e>$, which is an indication of the number of the Ni ions along the line of sight, is plotted in Fig.3 as a function of the total input power. The scaling with RF power is indeed observed, but the level of scatter in the data is quite large. This is not surprising because a number of additional parameters play a role when relating the level of Ni in the plasma to the influx from the FS. In particular, the Ni released from the FS is eventually re–deposited on limiters from where it can be sputtered by the normal processes(parallel energy flows in the SOL). In such a case, the Ni concentration cannot be related to the FS influx even if the Ni confinement in the plasma, as well as the degree of the Ni screening in the boundary, are known. The evidence for Ni migration and accumulation on the limiters, during the RF operation, is presented in Fig.4. Here the measure of the Ni concentration in the plasma during the ohmic phase, before the application of RF power, is plotted as a function of the pulse number. Note the general rise in Ni concentration with pulse number, as well as the tendency for the concentration to drop after several successive ohmic or low power pulses which effectively clean the limiters.

Much clearer information about the FS influx scaling can be obtained by studying

signals related directly to the influxes. Such an analysis[D'IPPOLITO 1990a] has been performed on the CrI data obtained during the operation of the Cr coated A_0 antenna. The analysis yields the scaling of the ICrI(intensity of CrI) with V_l. Here $V_l=Z_0(P_A/R_c)^{0.5}$ is the antenna line voltage(measured as maximum voltage across the transmission line), R_c is the corresponding coupling resistance, P_A is the power coupled by the antenna, and Z_0 is the characteristic impedance of the transmission line. Strictly speaking, V_l as defined here, is somewhat lower than the voltage across the current strap(or FS) of the antenna. This distinction is important for the theoretical model and is discussed further in Section 6.

Recently, Be–gettering was used in JET to improve the general impurity levels[THOMAS 1990]. During RF pulses the Be influx was monitored by means of the radiance of the BeI(4573 Å) line. The first results suggested[BUREŠ 1990b] a scaling $IBeI \propto P_A$ during a series of discharges with the coupling resistance R_c kept approximately constant. The clarifying illustration that the FS influx depends on voltage rather than power is shown in Figs.5a and 5b. During this discharge, the coupling resistance R_c was modulated by the density transients resulting from sawtooth activity. Due to the large changes in R_c, the generator power was periodically limited, resulting in a periodic decrease of RF power. At the same time, the Be influx from the FS was periodically increasing. Taking the R_c variation into account a clean correlation with the voltage emerged. The additional fast IBeI transients, observed in the signal, are caused by edge density spikes.

3.5 FS influx dependence on phasing(k_{II} spectrum).

The first evidence of the benefit derived from the antenna phasing was observed during early 1986 operation. As discussed in the corresponding publications[JACQUINOT 1986, BUREŠ 1988a], the level of metals originating at the FS of two adjacent A_0 antennae, Ni and Cr, was reduced by factor ≈ 2 when the antennae were phased so as to emit the maximum power at $k_{II}=7\ m^{-1}$. However, the direct measurement of the ICrI suggested that the Cr influx per MW was roughly the same in both cases, i.e. independent of phasing.

How do we reconcile these observations? Originally, it was suggested that the enhanced diffusion of the plasma in front of the antennae is phasing dependent. Indeed, the plasma edge density and temperature profiles were modified with k_{II}=0 m^{-1} so as to increase the density at the screen. As shown later, this implies increased sputtering in the RF sheaths. With k_{II}=7 m^{-1} the FS density was much lower. The coupling resistance was also much lower(factor >3) and therefore the antenna voltage was higher by a factor $>3^{0.5}$. These two effects nearly compensated and the resulting influxes were comparable. The observed difference in the Cr and Ni content in the plasma resulted from the difference in the edge profiles and the coresponding degree of screening. With respect to the behaviour of the n_e and T_e edge profiles, the observed strong modification(k_{II}=0 m^{-1}) can be significantly reduced by the conditioning techniques, but the enhanced transport in the immediate vicinity of the FS is still observed in JET[TAGLE 1990] even in the case of a well conditioned machine.

An alternative explanation of these results, obtained for the A_o antenna, could be that the FS influx does not depend on the phasing but more Ni and Cr was sputtered from the limiters with k_{II}=0 m^{-1}. This would be due to having higher edge fields at locations far away from the antennae, because the k_{II}=0 m^{-1} component reflects from the resonance zone. This mechanism can explain a markedly k_{II} dependent content of Ni in the plasma when the limiters were polluted by redeposition of the Ni and Cr.

The influx measurements from the V–shaped A_1 antenna provided much clearer answers and, in particular, the Be influx from the Be–gettered FS provided strong evidence[BUREŠ 1990b] that

a) the FS influx for V–shaped screens is phasing dependent(larger influx in monople phasing) and

b) a large fraction of the FS front face is exposed to sputtering.

In Fig.6 the Be influx, signal is corrected for the background Bremsstrahlung, is shown as a function of the antenna voltage in the monopole and toroidal dipole phasing. The antenna

power was modulated to estimate the time scale of the signal response. As discussed in Section 6 below, the essential element, which can explain the observed difference, is the V–shaped geometry and the formation of the front–face RF sheaths in the monopole phasing.

3.6 FS influx dependence on screen material.

One way to eliminate the Ni influxes, used frequently on JET, was the carbonisation of the vessel including the FS. After the carbonisation the Ni concentration in the plasma would drop by an order of magnitude[BEHRINGER 1986b]. The previous levels were recovered after 20–50 RF discharges. Similar reduction of the Ni level was observed when a large amount of additional power was applied to heat the plasma resulting in the "carbon bloom" phenomenon[PASINI 1990]. The carbon fluxes, present in the vessel, provided in–situ carbonisation of the FS. After a long series of RF heated discharges the Ni would reappear again. An estimate of the Cr influx, from the noncarbonised FS of the A_0 antennae, was published earlier[BEHRINGER 1986b]. $\phi_{Cr}^{FS}=10^{20}$atoms $MW^{-1}s^{-1}$ from the effective area $A_{FS} \approx 1m^2$ was derived. The rather high influx can not be explained by the deuterium sputtering alone but, as discussed below, the sputtering by light impurities and self–sputtering play the dominant roles. Therefore a screen material with a low self–sputtering coefficient should give a correspondingly lower influx. This was indeed observed with the Be gettered A_1 screens. Based on the hypothesis of the Be layer erosion[BUREŠ 1990b] the influx in monopole phasing was estimated to be $\phi_{Be}^{FS} \approx (1–2.5)x10^{19}$atoms $MW^{-1}s^{-1}$, a reduction by a factor ≈4–10. The entire surface of the FS of the A_1 antenna is ≈1 m^2. In Section 4.2 we provide an estimate of the Be influxes, from the same series of discharges, based on the VUV measurements of the Be concentrations in the plasma. The suitable choice of the FS material should depend crucially on its sputtering properties. The sputtering yields by D, O, C and self–sputtering should be well below one in the range of energies 0–1keV.

3.7 FS influx dependence on the plasma edge density.

To sputter the material from the FS, the density has to be finite at the surface facing the plasma. In order that enhanced sputtering in the RF sheath can take place, the density has to exceed the threshold value $\approx 10^{15}$ m^{-3}[D'IPPOLITO 1990a]. The first clear evidence of the FS influx dependence on the plasma density was found for the Cr influx from the A_0 antenna and the Be influx from the A_1 antenna. In the case of the Cr, the influx was found[D'IPPOLITO 1990a] to scale with the line integrated density measured along a vertical cord approximately 20 cm inside the plasma. Similarly, the Be influx was found to depend on the volume averaged density[BUREŠ 1990b], this dependence implicitly implying a scaling with the edge density. A direct comparison with the Cr data could not be made because the line density data were not available in the latter experiments. The two quantities are closely correlated and therefore the same trends of the influx behaviour are expected. To assess the influx behaviour in detail, the local density at the surface of the FS should be known. Such measurements proved to be difficult and only a limited amount of data exists[TAGLE 1990].

There are number of processes which can control the density at the FS. First, it will scale with the density at the ATTS which, in turn, depends on the volume averaged density, total RF power, recycling etc. In particular the level of the gas desorption from the limiter and wall is important. Second, RF induced diffusion in front of the FS can modify the local density at the screen.

Later, in Section 4.2, the measurements by the Langmuir probes in the antenna protection tiles[BRINKSCHULTE 1986] will be used to estimate the influx scaling. Because the above mentioned desorption, diffusion and the resulting FS density depend on the antenna voltage, the density and voltage scaling can not be separated in a straight–forward fashion.

3.8 FS influx dependence on general level of impurities.

The previously quoted Cr influx can be understood only if impurities contribute to the sputtering of the FS. The deuterium alone could not explain the results unless large fluxes at the maximum yield are involved in the sputtering process. Such D fluxes are not consistent with the calibrated D_α measurements. It was suggested by D'IPPOLITO et al.(1990a) that C, which is the dominant impurity during the operation with the C–belt limiters, is involved in the sputtering process. Indeed, C sputtering and the Cr self–sputtering can account for the measured Cr influx[D'Ippolito 1990a]. Recently, the C–belt limiters were replaced by Be–belt limiters. As a result C was replaced by Be as the dominant impurity. The influxes from Be–gettered A_1 antenna screens, with both the C and Be–belt limiters, were measured. In the case of Be–belt limiters the Be influx from the FS is reduced(compare Figs.6,7). Because the sputtering yields C –> Be and Be –> Be are comparable the difference in the influx could be attributed to the general level of impurities being lower in the latter case. Another contributing factor to the reduction of the FS flux might be a lower density at the ATTS due to the strong deuterium pumping by the Be[THOMAS 1990, BUREŠ 1990c]. Unfortunately the edge data supporting this claim do not exist, but the possibility of a strong reduction of the edge density in the Be environment will be discussed in more detail in Sections 4.3 and 6.

4.0 Be influx from the Be–gettered FS.

4.1 Experimental method.

Be was introduced into the JET device in two stages consisting of 1)Be–gettering of the vessel interior with the C–belt limiters and 2)Be–gettering of the vessel with the new Be–belt limiters. During both experimental stages the Be influxes from the FS were measured by monitoring IBeI. The preliminary results from the first stage were reported earlier[BUREŠ 1990b]. To correlate the IBeI to the Be neutral flux the number of ionisations per excitation(photon efficiency $S(T_e, n_e)$), for the experimental range of the

edge densities and temperatures, has to be known. In Fig.8 the photon efficiency of the BeI line is presented for a wide range of plasma parameters. The shaded area indicates the experimental range as obtained from the Langmuir probe data. Fig.9 shows IBeI as a function of the corrected signal $S(T_e, n_e)$IBeI. We find that the deviation from the IBeI signal, introduced by the correction, is well within the experimental error bar on IBeI as well as the Langmuir probe data. Therefore both the corrected and raw signals are equally representative of the influx. The contribution of the background Bremsstrahlung is correctly subtracted. Typically it amounts to $\leq$ 20% ot the total signal. One uncertainty remains unresolved. To relate IBeI to the neutral flux not only n_{edge} and T_{edge} must be known but also the fraction of Be atoms in their metastable states. The latter effect might introduce some additional density dependence which is not included in the present analysis. Measurements are not available to clarify this latter point. However theoretical investigations by SUMMERS(1990) relate the metastable fraction of the total neutral Be flux to the dynamic ionisation and thence to the local electron temperature. These results indicate that for T_{edge}>25 eV, the metastable fraction is reduced.

To understand the sputtering process at the FS, the voltage and density dependence of the ϕ^{FS} should be studied independently. This is not possible because the density at the FS, n_e^{FS}, is a function of RF power. There are two important processes, briefly mentioned in Section 3.7, which can influence n_e^{FS}; the enhanced diffusion in front of the FS and the deuterium desorption due to the heating of limiters. These were found to depend on the conditioning. Consequently, estimates of n_e^{FS} require measurements directly at the FS. The desorption process depends also on the limiter material, the amount of implanted gas and the total amount of the power, P_{II}, interacting with the limiters and wall.

While measurements of n_e^{FS} were not normally available, an estimate of density at the ATTS could be derived from an analysis of Langmuir probe data. The Langmuir probes were installed in the protection tiles of two of the antennae and the data represent the behaviour of the plasma edge density, temperature and their profiles. Because most of the

discharges were of the "Monster"[CAMPBELL 1988] type with the stabilised sawteeth, the Langmuir probe data proved to be of higher than usual quality. In a sawteething discharge the plasma edge parameters are strongly fluctuating as a result of the heat pulse, associated with the sawtooth collapse, reaching the plasma edge.

Generally the density at the ATTS is a function of the total RF power P_{RF}^{TOT}. The RF system was operated so as to keep the RF power on all antennae approximately equal. This is important because IBeI was monitored at the antenna 3D while the Langmuir probe data were collected at the antenna 1D. Thus $P_{RF}^{3D}/P_{RF}^{1D} = 0.85 \pm 0.1$ and $P_{RF}^{3D}/P_{RF}^{TOT} = 0.15 \pm 0.04$. From the Langmuir probes results n_e^{ATTS} can be expressed in form

$$n_e^{ATTS}[10^{18}\ m^{-3}] = 0.3 + 0.3(P_{RF}^{TOT}[MW])^{0.95} \qquad (1)$$

The characteristic e–folding length associated with the n_e profile is $\lambda_n = 1.8 \pm 0.5$ cm and does not depend on P_{RF}^{TOT}. This λ_n is characteristic of the main SOL. The profile characteristics right in front of the FS, in the "private" antenna SOL, are not known. Later in Section 4.3, when simulating the measured ϕ^{FS}, the change of this particular parameter with the antenna voltage has to be assumed.

The edge temperature also increases with RF power but somewhat slower. The scatter in the data is much larger, when compared to the density, and the best fit can be written in the form

$$T_e^{ATTS}[eV] = 25 + 4.0(P_{RF}^{TOT}[MW])^{0.75}. \qquad (2)$$

The corresponding temperature scale length in the main SOL is $\lambda_T = 4 \pm 2$ cm.

4.2 Behaviour of Be influx from the Be–gettered FS in JET with carbon belt limiters.

During the experimental campaign with the Be–gettered FS and the C–belt limiters the

Be signal monitoring the FS influx decays as a function of the number of Joules radiated through the FS. If the decay is attributed to the erosion of the Be layer the influx can be estimated(see Section 3.6). During a similar campaign with the Be–belt limiters the decay of the signal is not observed. This suggests that the Be–erosion is compensated by Be redeposition. If this assumption is valid, then at least part of the decay observed with the C–belt limiters could be due to the deposition of C on the FS.

In this Section we estimate the FS influx from independent measurements of the Be concentrations in the core plasma. These are derived from the calibrated intensities of the BeIV line(75.93 A). The conservation equation which relates the number of the Be ions in the plasma, originating at the FS, to the Be influx from the FS reads

$$\frac{N_{Be}^{FS}}{\tau_{Be}} = (1-\eta)\phi_{Be}^{FS} \qquad [MW^{-1}s^{-1}] \tag{3}$$

Here N_{Be}^{FS} $[MW^{-1}]$ is the total number of ions per MW of RF power which have the FS as their source. We define the total flux of the Be atoms originating at the FS of all eight antennas

$$\phi_{Be}^{FS,T} = \phi_{Be}^{FS} P_{RF}^{TOT} \qquad [s^{-1}] \tag{4}$$

where ϕ_{Be}^{FS} $[MW^{-1}\ s^{-1}]$ is the flux per MWs. As in the case of the A_o antenna, the corresponding area of the FS is $A_{FS} \approx 1\ m^2$. η is the screening efficiency which can be expressed in the form

$$\eta = 1 - \frac{n_n^{LCMS}}{n_n^{FS}} \qquad (5)$$

where n_n^{LMCS} is the density of the Be neutrals at the last closed magnetic surface(LCMS) and n_n^{FS} is their density at the FS. τ_{Be} is the global Be confinement time defined at the LCMS. The procedures to estimate N_{Be}^{FS}, τ_{Be} and η are described in detail in the Appendices. The same series of discharges is used in the analysis as in the case of the estimates based on the hypothesis of the Be layer erosion. Knowing the quantities N_{Be}^{FS}, τ_{Be} and η the Be influx can be calculated from Eq.(3). It becomes, for the monopole(k_{II} =0 m^{-1}) phasing, ϕ_{Be}^{FS} =(3 ± 1)x10^{19} atoms $MW^{-1}s^{-1}$ and compares favourably with the previously derived influx quoted in Section 3.6. For the estimate of the neutral Be screening the Langmuir probe data were used. The quoted error bar relates to the experimental uncertainties. An additional uncertainty is introduced when the influx is extrapolated to large powers and to very different operational scenarios.

The Be influx depends strongly on the density at the FS. The screening is also very sensitive to the absolute value of the edge density and its profile. In general these two dependencies tend to compensate each other.

How important is the Be influx from the FS in terms of the ion dilution in the plasma? Assume that the electron density can be written in the form

$$n_e = n_D + n_I Z_I + n_{Be}^{FS} Z_{Be} \qquad (6)$$

where $n_I Z_I$ represents the dominant impurity originating at the limiter and n_{Be}^{FS} Z_{Be} accounts for the fraction of electrons due to the FS. Then the contribution to Z_{eff} per MW of RF power is expressed

$$\delta Z_{eff} = \frac{N_{Be}^{SCR} Z_{Be}(Z_{Be} - 1)}{N_e} \qquad (7)$$

where $N_e = <n_e>V$ and V is the plasma volume. Taking the value $N_{Be}^{FS} \approx 2.5x10^{18}$ions MW^{-1}(Appendix A1) and the corresponding $N_e \approx 3.1x10^{21}$, we find that $\delta Z_{eff} \approx 0.01$ $[MW^{-1}]$. This value is a factor ≈ 2 lower than derived previously[BURES 1990b] because it takes into account the SOL screening.

One way to study the ϕ_{Be}^{FS} scaling is to use regression analysis. In Fig.10 the IBeI is plotted as a function of $F = c^{te}(V_{3D})^{\alpha} (P_{RF}^{TOT})^{\beta} s^{-\gamma}$. Here, s is the number of plasma pulses after the Be evaporation and the negative exponent indicates the decay of the signal partly due to the Be–layer erosion and partly due to the deposition of C. Even though n_e^{ATTS} is known, it appears that a more precise regression is obtained using P_{RF}^{TOT}, assuming that $n_e^{ATTS} \propto P_{RF}^{TOT}$. This can be understood in terms of the scatter in the n_e^{ATTS} data set introduced by the profile extrapolation from the measurements at two radial points. The values of the various exponents obtained in the regression analysis are $\alpha = 0.9 \pm 0.28$, $\beta = 0.85 \pm 0.12$ and $\gamma = -0.2 \pm 0.02$. The antenna voltage V_{3D} is related to the power coupled by the 3D antenna through the coupling resistance as defined in Section 3.4. The coupling resistance ($k_{II} = 0\ m^{-1}$) does not vary appreciably during the entire series of shots.This allows us,using $P_{3D}/P_{RF}^{TOT} \approx c^{te}$, to express the dependence of ϕ_{Be}^{FS} on voltage, e.g., $\phi_{Be}^{FS} \propto (V_{3D})^{\delta}$, and $\delta = \alpha + 2\beta = 0.9 + 1.7 = 2.6$. The value of the exponent $\delta = 2.6$ is typical of the conditions with the C–belt limiters. The ϕ_{Be}^{FS} dependence on voltage has to be primarily understood in terms of the n_e^{FS} evolution as a function of voltage. In this particular case, the stronger than linear($2\beta \approx 1.7$) dependence is a result of gas desorption and the corresponding edge density increase. The remaining, $\approx$ linear($\alpha \approx 0.9$), dependence is due to a combination of enhanced diffusion in the "private SOL" in front of the FS, weak dependence of the Be sputtering yield on voltage and some increase of

the C density. It is clear that the total exponent δ can depend sensitively on the state of the tokamak and some additional parameters like the plasma–antenna distance (LCMS–ATTS), plasma shape in front of the antenna etc.(See also the discussion in Sec.6). The exponent δ might change at high total power levels as a result of the saturation of the deuterium desorption.

4.3 Behaviour of Be–influx from the Be–gettered FS in JET with Be–belt limiters.

During the experimental period with the Be–belt limiters the behaviour of the Be influxes from the FS was different. The signal was relatively weaker and did not decay as a function of the coupled RF energy. As suggested in the previous Section, this implies a redeposition of the Be on the FS.

The bulk plasma density behaviour in these discharges is dominated by the strong deuterium pumping with the recycling coefficient $R_D<0.9$ during the entire RF pulse[BUREŠ 1990c]. A moderate amount of gas $\phi_g \approx 3x10^{21}s^{-1}$ was puffed into the plasma boundary to avoid an excessive drop in the plasma density. Unfortunately, during these discharges, Langmuir probe data were not available. In view of the complicated density behaviour it is not surprising that a regression analysis of the ϕ_{Be}^{FS} does not show any correlation with the volume averaged density $<n_e>$. In fact, with the present JET gas introduction system, it was not possible to reach a density steady–state during RF heating. In Fig.11 the IBeI signal is plotted as a function of $F=c^{te}(V_{3D})^{\alpha}$ for both the monopole and toroidal dipole antenna configurations. An exponent of $\alpha = 1.95 \pm 0.25$ was obtained from the regression analysis performed on the monopole phasing data. It can be concluded that, in toroidal dipole phasing, the influx ϕ_{Be}^{FS} is practically eliminated. The scaling law $\phi_{Be}^{FS} \propto (V_{3D})^{1.95}$ should be compared with the scaling in the C–belt limiter case(exponent 2.6). It is plausible to assume, on the basis of experimental observations, that there are two aspects of the weaker voltage dependence. First, the edge density does not increase with P_{RF}^{TOT} as strongly as with C–limiters. Second, the background level of impurities is lower.

In Fig.12, the influxes for both the C– and Be–limiter cases with monopole phasing are plotted as a function of antenna line voltage V_l. The IBeI data for the C–limiter case was normalized to the value ϕ_{Be}^{FS}= 2 x 10^{19} atoms MW^{-1} s^{-1}, which is consistent with both the erosion estimate of Sec.3.6 and the global particle balance estimate of Sec.4.2. The data referring to the C–limiter are corrected for the decay of signal as a function of pulse number s. At a voltage $V_l \approx$ 18 kV(corresponding to $P_A \approx$ 1 MW) the influx for the Be–limiter case is reduced by a factor $\geq$ 2 compared with the C–limiter case.. We conclude that the numbers for ϕ_{Be}^{FS} [$MW^{-1}s^{-1}$] and δZ_{eff} [MW^{-1}] quoted in the previous section for C–limiter are reduced by more than a factor of 2 when Be limiters are employed. The solid curves in Fig.12 represent the model simulations and are discussed in Sec.6.

5.0 Nickel influx from Be–gettered FS.

The Be–gettering does not deposit a Be film on surfaces which are not directly "seen" by the Be–getter heads. While the front face of the FS is covered by a Be layer, the surfaces in gaps of the FS have very small or no Be coverage at all. Therefore an influx of Ni is expected even when the FS is Be–gettered. For the same FS material, the influx from the gaps should be relatively less important than the influx originating at the front face[D'Ippolito 1990b]. The influx from the gaps is expected from theory to depend only very weakly on antenna phasing. In Fig.13 the signal INiXXV is shown for the cases of monopole and toroidal dipole phasing. Both discharges were run at similar densities, electron and ion temperatures and similar RF powers. As expected, no appreciable difference is noticed.

It is difficult to quantify the Ni influxes because no suitable spectroscopic line(low ionisation state monitoring the FS) exists. However, an estimate based on the Ni concentration in the plasma, confinement time and the neutral Ni screening can be made in a similar fashion as for the Be(see Appendix). There are two independent measurements of

the Ni concentration. The first is based on the VUV intensities of the NiXXV and NiXXVI lines and the second comes from the intensity of the Ni^{+26}(1.5886 Å) x–ray line. The latter is routinely used to derive the central ion temperature. The two methods agree within a factor of 2–3, but some cases exist where the discrepancy is larger. The detailed Ni behaviour will be treated in a separate publication. In particular the Ni migration from the FS to the belt limiters and subsequent sputtering by various mechanisms will be discussed. Here we estimate the influx immediately after the Be–gettering and after a relatively small number of RF shots. Under these conditions the contamination of limiters and the antenna protection tiles should not be too important. This is indeed the case because the Ni^{+26} photon count rate, in the ohmic phase of the discharges studied, is very low. Taking the uncertainties in the estimates of the Ni concentration and confinement into account, the influx from the gaps of the FS for the C–limiter case can be estimated as $\phi_{Ni}^{FS,gap} \approx 1–4 \times 10^{18}$ atoms $MW^{-1}s^{-1}$. This assumes that the FS is the only source of Ni, which is actually not the case, so this estimate is only approximate. The contribution of Ni to Z_{eff} is, in these discharges, very small. How do we reconcile these observations with the previously observed high Cr influxes from the A_0 antenna? First, the characteristic dimension δs of the A_0 "private SOL" was ≈ 50% of the corresponding δs of the A_1 antenna(see Fig.1). Second, the influx originating in the gap is much smaller than the influx coming from the front face of the FS, which gave the dominant contribution to the influx from the A_0 screens.

6.0 Theoretical model.

The formation of Bohm–Debye sheaths on the limiters, wall and other surfaces in contact with the plasma is the dominant mechanism of the physical sputtering by the plasma and impurity ions. As mentioned in Sec.1.0, this process leads to a "global" impurity influx associated with the RF power flow into the SOL. This process is not sufficient to account for the observed impurity influx from the FS of powered

ICRF antennae. In a recent paper, PERKINS(1989) suggested that the impurity release from the screen could be explained by enhanced sputtering due to ion acceleration in the RF sheaths which form along magnetic field lines connecting the two surfaces of the FS gap. The pshysics of the gap sheaths has been studied in several other recent papers[MYRA 1990, D'IPPOLITO 1990a, CHODURA 1990]. However, the formation of RF–enhanced sheaths is expected to occur on other surfaces as well. In D'IPPOLITO(1990b) and in the present section, the treatment of RF sheaths is extended to include front face sheaths on the V–shaped FS of the type used in the A_1 antennae(see Fig.14). Generally speaking, whenever a substantial RF flux is linked by the magnetic fields connecting two conducting surfaces(thereby forming a complete circuit), RF sheaths will form at the points of contact with the surface, giving a potential drop across the sheath on the order of the induced voltage across the magnetic filed line segment. This voltage is typically much larger than the electron temperature which characterizes the potential drop of the Debye sheath. The RF sheath therefore leads to a greatly enhanced sputtering from the FS when the antenna is activated.

A complete sputtering model requires a quantitative treatment of the particle inventory in the vicinity of the FS because i)the sputtering yields are sensitive to the masses and charges of the incoming particles; ii)the degree of self–sputtering depends on the local ionization and therefore on the electron density; and iii)the RF sheath potential is also sensitive to the local electron density[MYRA 1990]. A theoretical model has been developed which includes the physics of radial transport, ion acoustic flow along field lines, neutral free streaming, ionization, and the sputtering and self–sputtering associated with both gap and front–face RF sheaths. A detailed description of the model is given in D'IPPOLITO(1990b) and only a brief summary of the main results of the calculation will be given here. The detailed comparisons given below, demonstrate that the model can reproduce the magnitudes of the measured influxes for the various JET antenna/limiter configurations and gives good qualitative agreement with observed dependence of the metal

impurities on antenna phasing and voltage, magnetic field angle with respect to the FS, and screen material. The role of oxygen and the general level of impurities can also be understood in the context of the model. Thus the model provides a useful framework for understanding and interpreting the experimental impurity influx data summarized in Secs. 3.0–5.0.

The model is restricted to two regions: the "private SOL", bounded by the surface we refer to as the ATTS, where field lines terminate in the antenna protection tiles(see Fig.14), and the "sputtering region" where the field lines intersect a surface of the FS. For simplicity, sputtering by only two species of ions diffusing in from the SOL is retained, the majority ions and one species of limiter impurity. The density and charge states of these ion species and the electron density are specified at the ATTS as inputs to the model and their radial profiles in the private SOL are calculated using the standard diffusion equation. The model includes the volume–averaged particle inventory equations for the FS neutral and ion species to give an accurate evaluation of the neutral impurity influx including self–sputtering by the FS impurity species. The electron density is determined by the quasi–neutrality condition including the contribution of the FS ions, and the FS ion density in turn depends on the electron density through ionization. Thus, the neutral influx is a highly nonlinear function of density in the regime where self–sputtering is important.

The main result of the theoretical model is the following expression[D'IPPOLITO 1990b] for the influx of the neutral metal impurities(atoms/cm^{2}s) from the screen towards the plasma:

$$\Gamma_{FS}^{(o)} = \frac{P_f^{(o)} \Sigma_j' \Gamma_j^{(o)}}{1 - A} \qquad (8)$$

where $P_f^{(o)}$ is the probability of a sputtered neutral atom reaching the SOL without either

sticking to another FS surface or ionizing in the sputtering zone, $\Gamma_j^{(o)}$ denotes the FS impurity influx due to the sputtering by ions of species j, and A is the neutral amplification factor due to self–sputtering by impurity ions(summed over all charge states). The prime denotes that the species summation does not include the FS ions, whose self–sputtering contribution is contained in the factor (1–A) in the denominator of Eq.(8). Note that when A approaches unity, the neutral influx becomes arbitrarily large in the model leading to an "avalanche" of metal impurities[D'IPPOLITO 1990a, 1990b]. The impurity influx $\Gamma_j^{(o)}$ is given by

$$\Gamma_j^{(o)} = (\bar{n}_{+f}\, c_{sf}\, Y \sin\Psi)_j \frac{A_{sp}}{A_{FS}} \qquad (9)$$

where $(\bar{n}_{+f})_j$ is the volume–averaged density of ion species j in the sputtering region, $(c_{sf})_j$ is the corresponding sound speed, Y_j is the sputtering yield of FS atoms for each incident ion species j, and the angle Ψ is defined between the magnetic field line and the tangent to the sputtering surface. Finally, A_{sp}/A_{FS} is the ratio of the area of the total sputtered FS to the entire area of the FS frame. Both Ψ and the area ration A_{sp}/A_{FS} are functions of the angle θ between the magnetic field and the Faraday screen. The RF sheath potential enters Eq.(9) through the functional dependence of the sputtering yield, $Y = Y(E,\Psi)$, where the sputtering energy $E = ZeV_{sh}$ and V_{sh} is the total time–averaged sheath potential taking into account both the rectified RF voltage and the contribution of the Debye sheath. As the geometric factors in the model and magnitude of V_{sh} differ for each sheath, the model is formulated separately for the gap and the front face sheath, as discussed in detail in the theoretical paper.

The key physical quantities which determine the predicted influx $\Gamma_{FS}^{(o)}$ are the local electron and ion densities at the FS and the driving voltage of the sheath. The species density at the screen depends on the assumed density at the ATTS, n_j^{ATTS}, the diffusion coefficient $D_\perp$, and the separation δs between the ATTS and the screen(see Fig.1). The

toroidally–averaged value $\delta s = 7$ mm for the front–face sheath model and $\delta s = 9$ mm for the gap sheath model in modeling the A_1 antennae; the choice of density and diffusion coefficient are discussed below. The driving voltage of the RF sheath is proportional to the antenna line voltage V_l and depends on the antenna phasing and on the specific sheath geometry(flux linkage), as discussed in detail in D'IPPOLITO(1990b). In the gap case, the driving voltage can be approximated as the total voltage along the FS(which is larger than the line voltage by a factor of about 2.6 for the A1 antennae) divided by the number of screen elements, and is only weakly dependent on the antenna phasing. For the front face sheath, the driving voltage in monopole phasing equals the gap voltage times the number of gaps spanned between field line connection points ($\approx$ 2–3 for JET) and thus typically dominates the sputtering. In toroidal dipole phasing, the driving voltage for front face sheaths vanishes by symmetry if the FS has the V–shaped indentation typical of the A_1 antennae(illustrated in Figs.1 and 14) leaving only the weaker gap sheath sputtering. This dramatic phasing dependence vanishes for flat screens of the A_0 type. Thus, the phasing dependence of the front face sheath model corresponds with experimental observations for the A_0 and A_1 antennae discussed in Sec. 3.5 and illustrated for the A_1 antenna Be influx data in Fig.11.

In preliminary comparisons of the model with experiment[D'IPPOLITO 1990b], the densities n_j^{ATTS}, the diffusion coefficient $D_\perp$, and the antenna line voltage V_l were treated as independent parameters. Even at this level of approximation, it was possible to establish that the influx predicted by the model roughly agreed with the measured influxes for the various A_0 and A_1 experimental situations outlined in Sec.2.0, given reasonable assumptions about the parameters. Morover, it was shown in that paper that the model's predictions agreed qualitatively with the experimental dependence on magnetic filed angle θ(discussed here in Sec.3.3) and antenna phasing(see Sec.3.5). An important conclusion from this comparison was that RF–enhanced diffusion was needed to achieve sufficient screen density to produce the observed impurity influx. Additional experimental evidence

on the limiter impurity fraction and the ATTS electron density was also illustrated in that paper[D'IPPOLITO 1990b], with an emphasis on the important role of self–sputtering at higher density.

In the present paper, we carry the comparison of theory and experiment further by incorporating models of the experimentally observed dependences of the SOL density and the RF–enhanced diffusion coefficient on the antenna voltage V_l. Our goal here is to account for the observed voltage dependence of the Be influx data with C and Be limiters shown in Fig.12. For purposes of this comparison, we convert the local flux $\Gamma_{FS}^{(o)}$(atoms/cm^2 s) into the total flux ϕ^{FS}(atoms/s) by multiplying by A_{FS}, the total surface area of the FS[to which $\Gamma_{FS}^{(o)}$ is normalised in Eq.(9)],

$$\phi^{FS} = \int\int \mathbf{dA}\cdot\Gamma_{FS}^{(o)} \approx \Gamma_{FS}^{(o)}\, A_{FS} \qquad (10)$$

and we use $A_{FS} = 0.9\ m^2$ for each FS in the A_1 JET antenna system.

In the numerical results presented here, the majority species is assumed to be deuterium and the notation A/B is adopted to indicate the choice of the remaining two ion species in the model(limiter impurity A and FS impurity B). For the C/Be case, we fix the carbon to electron density ratio at the ATTS to $n_c/n_e = 0.1$ and assume a typical charge state in the SOL of C^{+3}. As discussed in Sec.4.1, the density n_e^{ATTS} is a function of RF power through the processes of desorption and ionization. The empirical relation(1) can be expressed in terms of antenna line voltage as

$$n_e^{ATTS} = n_{e\,o}^{ATTS} + c_n P_o^{\nu} (V_l/V_o)^{2\nu} \qquad (11)$$

where $n_{e\,o}^{ATTS} = 3\text{x}10^{17} m^{-3}$, $c_n = 3 \text{ x } 10^{17} m^{-3}$, P_o[MW] = 8, V_o[kV] = 17 and $\nu = 0.95$. The scaling of $D_\perp(V_l)$ in the private SOL is not known experimentally. We used the scaling

$$D_{\perp} = D_o\,(1 + c_D(V_l/V_{ref})^{\mu}) \qquad (12)$$

with D_o = 1 $m^2 s^{-1}$(approximately Bohm diffusion using edge parameters), c_D = 2, and V_{ref}[kV] = 10. The choice of these parameters is constrained by the observation that the experimental flux ϕ_{Be}^{FS} is negligibly small as V_l–> 0 and has the estimated value ϕ_{Be}^{SCR}= 3 ± 1 x 10^{19}atoms $MW^{-1}s^{-1}$ at the voltage V_l = 18 kV corresponding to P_{RF} = 1 MW. Comparing the results of the model for diferent values of μ with the data, it was found that good agreement of the influxes was obtained with a linear scaling(μ = 1). We remark that a linear scaling in Eq.(12) is also consistent with the idea that RF–induced transport, most likely convective, near the screen is caused by E x B drifts associated with the spatial variation in the rectified RF sheath potential which should induce a large convective cell in front of the FS.

For the Be/Be case, the following changes in the parameters were made. The dominant limiter impurity was assumed to be Be^{+2}, because the ionization energy for the second state of Be is significantly higher than that for carbon. The impurity fraction was also reduced to n_{Be}/n_e = 0.05, motivated by the observed gettering of oxygen by Be limiters with consequent reduction in limiter sputtering. Also, the density parameter ν in Eq.(11) was reduced to ν = 0.7 to model the deuterium pumping by the Be limiters (discussed in Sec.4.3).

The results of the model calculation of $\Gamma_{FS}^{(o)}$ versus V_l for the C/Be and Be/Be cases are shown in Fig.12 with the most important physical parameters chosen as discussed in this section. The other parameters in the model(not discussed in detail here) were chosen as in the earlier paper[see Sec.4.B of D'IPPOLITO 1990b]. Only the front face sputtering contribution was included, because the coverage of the gap surfaces by the evaporated Be is thought to be small. It is important to note that the spectroscopic Be influx data is illustrated in Fig.12 for the normalization ϕ_{Be}^{FS} = 2 x 10^{19} atoms MW^{-1} s^{-1}, which represents a good compromise between the two experimental methods used to estimate the

influx(the erosion rate estimate in Sec.3.6 and the global particle balance estimate in Sec.4.2). With this normalization, the theoretical and experimental influx estimates show excellent agreement over a wide range of antenna volltages. However, it should be kept in mind that the error bars on both the theoretical and experimental influx estimates are substantial. Due to uncertainties in the inputs to the model and in the calibration of the data, agreement of the influxes to within a factor of two is considered good. Even taking the upper limit of the estimate of Sec.4.2, $\phi_{Be}^{FS} = 4 \times 10^{19}$ atoms $MW^{-1}s^{-1}$, we find that the agreement between theory and the data can be considered satisfactory.

The most important aspect of the model is that it reproduces the relative difference between the C and Be limiter data, given reasonable assumption about the RF and SOL parameters. This suggests that the basic physics of the model is correct. The fact that the model curves also reproduce the voltage dependence of the data indicates that the assumed relationship between the antenna voltage, edge density and the SOL diffusion coefficient are reasonably accurate. Thus, we have used the data and the model together to infer that the voltage dependence of the experimental influx in JET is due primarily to the increase in edge density with RF power(determined from probe data) and to the increase in the local diffusion coefficient(characterizing the convective process) with RF voltage. The sputtering yield of Be is insensitive to energy(and hence to RF voltage) in the range corresponding to Fig.12.

Another possible point of comparison between theory and experiment is the Ni influx from the gap during the Be evaporation experiments with carbon limiters. The experimental estimate of the Ni influx from the gap given in Sec.5.0 yields $1 - 4 \times 10^{18}$ atoms s^{-1} at a power level of 1 MW. The corresponding theoretical value(assuming monopole phasing, $V_l = 17$ kV, and $A_{FS} = 0.9$ m^2) is 5.8×10^{18} atoms s^{-1}, which is within a factor of two of the high end of the experimental estimate. The two results would be consistent if we assume 50% coverage of the sputtering surface in the gap by the evaporated Be. This is not unreasonable because of the "rounded–T" shape of the FS bars,

which allows some line of sight from the plasma to the gap sputtering surface.

Finally, in Fig.15 we use the model to illustrate both the phasing dependence and the sensitivity to FS material of the impurity influx from the JET A_1 antennae. Three cases are illustrated: (a) monopole operation with C limiters and Ni screens **without** Be evaporation; (b)monopole operation with Be limiters and Be screens; and (c) dipole operation with Be limiters and Be screens. For completeness, the gap sputtering contributions are retained in all three cases; as noted above, in dipole phasing, the gap contribution constitutes the entire FS flux. The parameters for the C/Ni case are chosen as in the C/Be case of Fig.12 except that $n_c/n_e = 0.15$ is used to model the higher level of C observed in the absence of Be evaporation(probably due to limiter sputtering by O), and Ni sputtering and ionization data is used for the screen impurity. The parameters for cases (b) and (c) are identical to that of the Be/Be case of Fig.12, except that in case (c) toroidal dipole phasing is assumed. Comparing curves (a) and (b) in Fig.15 clearly shows the advantage of Be as a screen and limiter material. One important reason for this is the reduced self–sputtering coefficient for the Be screen. At $V_1 = 25$ kV, the Ni influx is enhanced due to self–sputtering by approximately a factor of 2(i.e. the neutral amplification factor $A \approx 0.5$). Curves (b) and (c) show the dependence of the influx on the antenna phasing. The Be influx is greatly reduced in dipole phasing for the A_1 antennae because the RF voltage driving the front face sheath vanishes by symmetry, leaving only the much smaller gap sputtering contribution.

7.0 Conclusions.

During ICRF heating in JET, local metallic influxes from the FS of RF antennae are usually observed. The FS influxes depend strongly on the antenna voltage and the FS density. In general, these two parameters are coupled through the power dependent gas desorption processes and the enhanced diffusion/convection in front of the FS. Both tend to increase the density at the surface of the FS. These two dependences and the additional

observed dependences on the magnetic field versus FS angle, antenna phasing, FS geometry and FS material are consistent with the sputtering processes in the RF enhanced Bohm–Debye sheaths. Such sheaths will form at the surfaces connected by the magnetic field lines linking a substantial RF magnetic flux. In the case of JET antennae, RF sheaths will form in the gaps of the FS and, in particular, at the front face of the V–shaped FS of the A_1 antenna. The V–shaped FS allows for a larger separation ATTS–FS when compared to the flat front face(A_0 antenna). The A_1 front face sputtering is sensitive to the antenna phasing and, in the toroidal dipole, the influx is reduced to a very low, practically negligible level since the RF flux driving front face sheaths nearly vanishes in this phasing. In monopole phasing the front face Ni influx is eliminated by the Be–gettering. An additional benefit from Be–gettering is derived from the reduced background impurity level. During the operation period with the C–belt limiters and Be–gettering the FS influx(in monopole phasing) can be estimated as $\phi_{Be}^{FS}=3 \pm 1 \times 10^{19}$ atoms MW^{-1} s^{-1}. At the same time the Ni influx from the FS gaps is in the range 1–4 x 10^{18} atoms MW^{-1} s^{-1}. The resulting contribution to Z_{eff} is $\delta Z_{eff}/P_{RF}$ <0.015 MW^{-1}, which is somewhat lower than the previous estimate[BUREŠ 1990b] because the screening of neutral atoms in the SOL is now properly accounted for. The contribution to Z_{eff} from the FS influxes in Be case is very low not only because the influx is substantially reduced but also because the charge number of Be is low. The derived front face influx ϕ_{Be}^{FS}compares favourably with the estimate based on the hypothesis of the FS erosion(see Section 3.6). During the operation period with the Be–belt limiters the numbers quoted above are reduced by more than a factor of 2. The fact that the FS influxes are small, even in monopole phasing, is confirmed by the global measurements of Z_{eff} and radiated power P_{rad}. It should be kept in mind that the FS influxes are low in JET because a number of necessary conditions are met: Be is a material with a low self–sputtering coefficient; the FS elements are at small angle with respect to the magnetic field; the RF power density and therefore the antenna voltage are reasonably low; and, the background impurity level and

FS density are also low. If any of these requirements are violated the influxes need not remain negligible, and the process of gradual limiter pollution may take place. Then the metallic impurities, which originally came from the screen, can be sputtered by the "normal", power linked processes. On smaller devices, with low RF wave absorption per pass, the distinction between the influxes associated with the RF field and those associated with RF power cannot be easily made, and the impurity influx due to the RF power appearing in the SOL might be mistakenly attributed to some exotic RF wave phenomenon.

In recent experiments on JET the Ni FS were replaced by the Be FS and the Ni influx from the FS was completely eliminated. The preliminary conclusions indicate that in the dipole phasing the remaining Be influx from the FS gaps is indeed completely negligible. The total influx(from the front face and gaps), in monopole phasing, is low enough to allow for the successful coupling of large RF powers to H–mode plasmas. A detailed assessment of the Be screens on the JET antennae will be subject of a future report.

Acknowledgements.

We wish to thank our colleagues in the JET team, especially the tokamak operating teams and those operating the dignostics used in the experiments reported in this paper.

References.

BEHRINGER K. et al.(1986a) Contr. Fusion and Plasma Heating(Proc. 13th Europ. Conf. Schliersee) Vol.10C, Part I, Europ. Phys. Soc.p.176.

BEHRINGER K. et al.(1986b) Proc. 11th Int. Conf. on Plasma Phys. and Contr. Nucl. Fus. Res. Kyoto, Vol.1(IAEA, Vienna) I, p.197.

BEHRINGER K. et al.(1989) Plasma Phys. and Contr. Fusion, Vol.31, p.2059.

BUREŠ M. et al.(1988a) Plasma Phys. and Contr. Fusion, Vol.30, No.2 p.149.

BUREŠ M. et al.(1988b) Plasma Phys. and Contr. Fusion, Vol.30, No.13 p.1833.

BUREŠ M. et al.(1990a) Nucl. Fusion, Vol.30, No.2 p.251.

BUREŠ M. et al.(1990b) IAEA Tech. Comm. Meeting, Garching, published in Fusion Engrg. Des. 12 p.251.

BUREŠ M. et al.(1990c) 9th Int. PSI Conf.(Bournemouth), to appear in J. Nucl. Mat.

BRINKSCHULTE H. et al.(1986) Proc.13th Europ. Conf. on Contr. Fusion and Plasma Phys., Schliersee. Vol.10C, Part II, p.77.

CAMPBELL D.J. et al.(1988) Phys. Rev. Lett. 60, p.2148.

CHODURA R.(1990) IAEA Tech. Comm. Meeting, Garching, published in Fusion Engrg. Des. 12 p.111.

DENNE B. et al.(1985) Proc.12th Europ. Conf. on Contr. Fusion and Plasma Phys., Budapest. Vol.9F, Part I, p.379.

D'IPPOLITO D.A.et al.(1990a) IAEA Tech. Comm. Meeting, Garching, published in Fusion Engrg. Des. 12 p.209.

D'IPPOLITO et al.(1990b) submitted to Plasma Phys. and Contr. Fusion.

FUJI T. et al.(1988) Proc 12th Int. Conf. on Plasma Phys. and Contr. Nucl. Fus. Res. Nice, IAEA–CN–50/E–2–4 (IAEA, Vienna).

HAWKES N. et al.(1989) Contr. Fusion and Plasma Heating(Proc. 16th Europ. Conf. Schliersee) Vol.13B, Part I, Europ. Phys. Soc.p.79.

HIGGINS M.J. et al.(1989) Culham Report CLM–R294.

JACQUINOT J. and JET TEAM.(1986) Proc. 11th Int. Conf. on Plasma Phys. and Contr. Nucl. Fus. Res. Kyoto, Vol.1(IAEA, Vienna) I, p.449.

JACQUINOT J. and JET TEAM(1988), Plasma Phys. and Contr.Fusion, Vol.30, No.11, p.1467.

JACQUINOT J. et al.(1990) IAEA Tech. Comm. Meeting, Garching, published in Fusion Engrg. Des. 12 p.245.

KAYE A.S. et al.(1985) Proc. 11th Symposium on Fusion Engineering, Austin, Texas. Vol.II, p.1204.

KAYE A.S. et al.(1987) Fusion Technology, Vol.2, p.203.

LENNON M.A. et al.(1986) Culham Report CLM–R270.

MYRA J.R. et al.(1990) Nucl. Fusion 30, p.845.

ODAJIMA K. et al.(1986) Proc 11th Int. Conf. on Plasma Phys. and Contr. Nucl. Fus. Res. Kyoto, Vol.1 (IAEA, Vienna) I, p.151.

PASINI.D.(1990) 9th Int. PSI Conf.(Bournemouth), to appear in J. Nucl. Mat.

PERKINS F.W.(1989) Nucl. Fusion 29, p.583.

STEINMETZ K. et al.(1989) Nucl. Fusion 29, p.277.

SUMMERS H.P. et al.(1990) to be submitted to Plasma Phys. and Contr. Fusion.

TAGLE J.A. et al.(1990) IAEA Tech. Comm. Meeting, Garching, published in Fusion Engrg. Des. 12 p.217.

THOMAS.P. and JET TEAM.(1990) 9th Int. PSI Conf.(Bournemouth), to appear in J. Nucl. Mat.

WEYNANTS R.R. et al.(1988) Proc 12th Int. Conf. on Plasma Phys. and Contr. Nucl. Fus. Res. Nice, IAEA–CN/E–2–1(IAEA, Vienna).

WILSON J.R. et al.(1988) Proc 12th Int. Conf. on Plasma Phys. and Contr. Nucl. Fus. Res. Nice, IAEA–CN–50/E–4–1(IAEA, Vienna).

APPENDIX.

A1. Estimate of the number of Be ions in the plasma originating at the FS.

The total number of Be ions in the plasma, during the RF pulse, N_{Be}^{TOT} is shown in Fig.16 together with the ohmic (N_{Be}^{Ω}) and RF (N_{Be}^{RF}) contributions, as a function of pulse number. The pulse # 19720 was the first discharge after a fresh Be–gettering. The N_{Be} quantities are defined:

$$N_{Be}^{TOT} = c_{Be} \langle n_e \rangle V \tag{A11}$$

$$N_{Be}^{RF} = N_{Be}^{TOT} - N_{Be}^{\Omega} \tag{A12}$$

Here $c_{Be} = \langle n_{Be} \rangle / \langle n_e \rangle$ is the Be concentration and V is the plasma volume. We note that the ohmic level N_{Be}^{Ω} decays with pulse number. This indicates that the Be–layer on the limiters is quickly eroded. N_{Be}^{RF} includes the Be ions in the plasma which are sputtered partly from the FS and partly from the Be covered C–limiters.

$$N_{Be}^{RF} = N_{Be}^{LIM} + N_{Be}^{FS,T} \tag{A13}$$

The general impurity behaviour during Be–gettering, with both the C and Be limiters, indicates that the dominant impurity in the plasma is that of the belt limiter material. It was found[BURES 1990a, b] that in both cases the effective charge scales as

$$(Z_{eff} - 1) = c^{te} \frac{P_{TOT}^{\epsilon\, i}}{\langle n_e \rangle} \quad i = C, Be \tag{A14}$$

where $P_{TOT} = P_{\Omega} + P_{RF}$, $\epsilon_C \cong 0.4$ and $\epsilon_{Be} \cong 0.55$. Expressing Z_{eff} in terms of the dominant impurity we derive

$$<n_I> = \frac{c^{te}}{Z_I(Z_I - 1)} P_{TOT}^{\epsilon_i} \qquad \text{(A15)}$$

Thus, assuming that the Be layer is sputtered from the C–belt limiters by the same process as from the Be–belt limiters, we can obtain N_{Be}^{LIM} in the form

$$N_{Be}^{LIM} = N_{Be}^{\Omega}(P_{TOT}/P_{\Omega})^{\epsilon_{Be}} \qquad \text{(A16)}$$

Usually the FS influx per MW is quoted in literature. It can be argued in a given case that another scaling(eg. voltage and density) might be more accurate. However, because in most cases an approximate scaling with the power is always found, we adopt the same normalisation here. In Fig.17 $N_{Be}^{FS} = N_{Be}^{FS,T}/P_{RF}^{TOT}$ is plotted as a function of pulse number. The signal shows a decay which is similar to that of the influx measured directly at the FS. This is encouraging because these two quantities should be directly related through the confinement and screening. In the inset the best fit to this decay (only D(H) discharges were considered) yields $N_{Be}^{FS} = (2.5 \pm 0.5)\text{x}10^{18}$ ions MW^{-1} in the plasma. The exponent of the decay(as a function of pulse number) is higher than in the case of the FS influx. That there is some difference is not too surprising given the error bar in the BeIV data and the estimate of N_{Be}^{LIM}.

A2. Estimate of the Be confinement in the plasma.

One way to estimate the global Be confinement time τ_{Be} is to measure the characteristic

decay time at the RF power switch–off. The e–folding time is a measure of the confinement if the influx is instantaneously switched–off. This is the case only for the influx from the FS. The influx coming from the belt limiter, which is comparable in the amplitude, continues to enter the plasma even after the RF power was switched–off due to the decay of the stored RF energy. Because the principal impurity originating at the limiter scales as $\approx P_{TOT}^{0.5}$, we assume that the corresponding influx can be expressed

$$\phi_{Be}^{LIM}(t) = \phi_{Be}^{LIM} \exp(-t/2\tau_{INC}^{E}) \qquad (A21)$$

The time decay of the N_{Be}^{RF}, which has two separate influx sources, can be shown to have the form

$$N_{Be}^{RF}(t) = \{N_{Be}^{RF} + \phi_{Be}^{LIM}\tau^{*}[1 - \exp(-t/\tau^{*})]\} \exp(-t/\tau_{Be}) \qquad (A22)$$

where $\tau^{*} = (2\tau_{INC}^{E}\ \tau_{Be}/(\tau_{Be} - \tau_{INC}^{E}))$ and $\tau_{INC}^{E} = \delta W/(P_{RF} - \delta P_{\Omega})$. Expressing $\phi_{Be}^{LIM} = N_{Be}/\tau_{Be}$, Eq.A22 can be fitted to a particular decay, as shown in Fig.18, yielding a best fit confinement time $\tau_{Be} = 0.2–0.25$ s. The pertinent incremental energy confinement time is $\tau_{INC}^{E} = 0.42$ s. Note that in Fig.18 the Be density $\langle n_{Be} \rangle^{TOT} = N_{Be}^{TOT}/V$ is plotted. It has the same time evolution as N_{Be}^{RF} in Eq.22 because the plasma volume does not change during the time shown in the figure. The Be confinement time obtained by the method described here is in the same range as the impurity confinement times previously observed on JET by more sophisticated methods[HAWKES 1989].

A3. Estimate of Be screening.

In order to relate the FS influx to the influx across the plasma boundary(LCMS) we have to calculate the degree of screening. Consider the Be neutrals, after being sputtered, streaming across the "private SOL" of the antenna and then across the main SOL. We will

calculate the neutral Be decay due to ionisation and assume that only the remaining neutrals enter the plasma. Those which are ionised before reaching the LCMS will be assumed to be completely screened–off. The conservation of the Be neutrals, in steady–state, is written

$$-\mathrm{div}(n_n \vec{v}_n) = n_e n_n \xi_i \qquad \text{(A31)}$$

ξ_i is the ionisation rate as defined in Ref.[LENNON 1986, HIGGINS 1989]. We assume that ξ_i does not vary appreciably across the ionisation regions. Assuming poloidal and toroidal symmetry and the exponential electron density decay, with e–folding lengths $\lambda_n^{(1)}$and $\lambda_n^{(2)}$(index 2 refers to the main SOL), the neutral Be density at the LCMS can be expressed

$$n_n^{LCMS} = n_n^{FS} \exp\{ - \frac{\xi_i^{(2)} \lambda_n^{(2)}}{v_n} [n_e^{LCMS} - n_e^{ATTS}] - \frac{\xi_i^{(1)} \lambda_n^{(1)}}{v_n} [n_e^{ATTS} - n_e^{SCR}] \} \qquad \text{(A32)}$$

Here n_e^{ATTS} and n_e^{FS} are the electron densities at the ATTS(defined in Section 3.7) and the FS and v_n is the Be neutral velocity at which the neutrals are released, which corresponds to a typical energy of 1 eV. Values of ξ_i and λ_n are based on the Langmuir probe measurements. For the discharge shown in Fig.18, $n_n^{LCMS}/n_n^{FS} \approx 0.4$, implying a screening efficiency $\eta \approx 0.6$. The estimate of screening in the "private SOL" does not account for the enhanced diffusion. This is a reasonable assumption because the major part of the ionisation takes place in the main SOL.

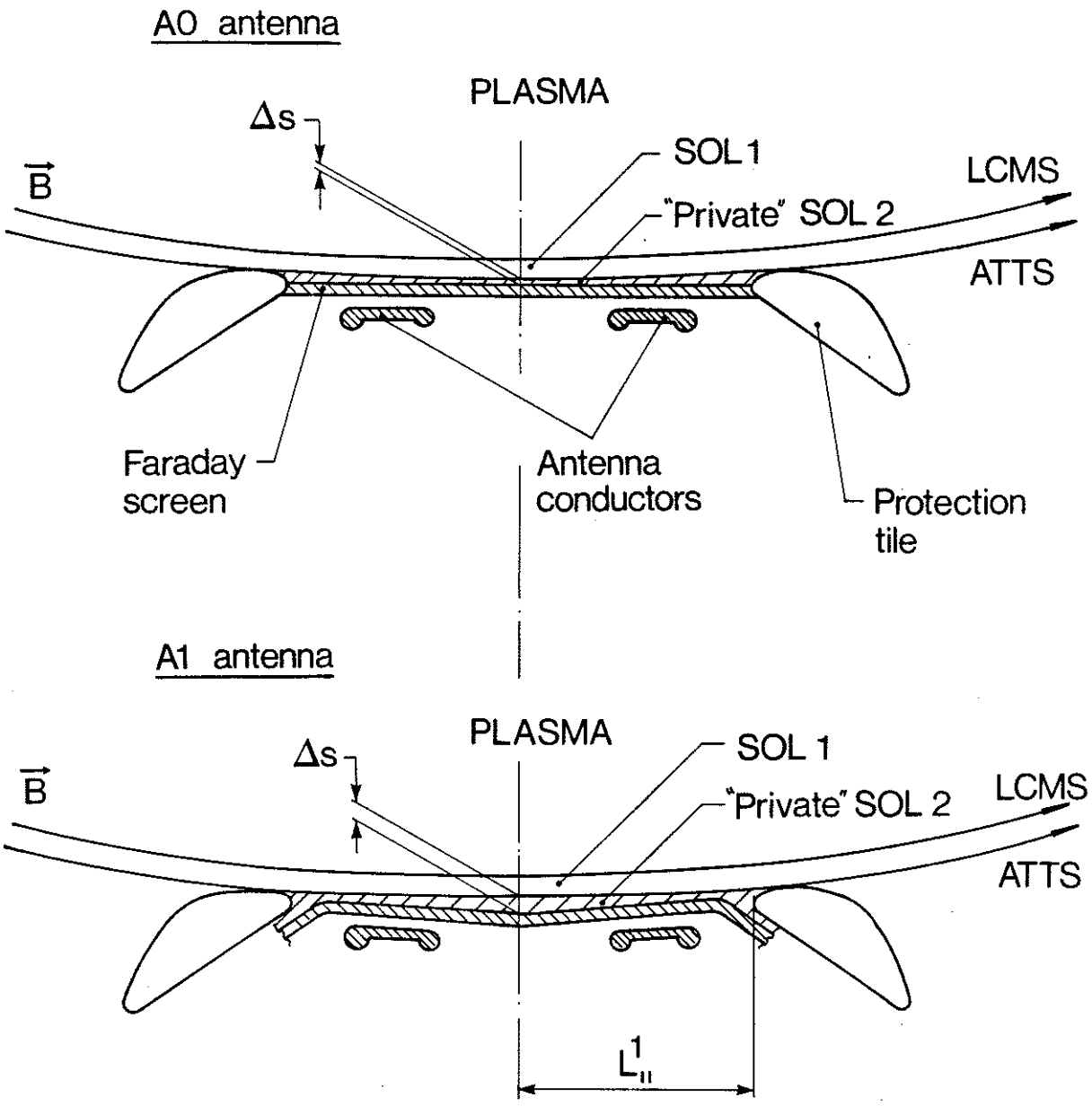

Fig.1. Schematic drawing of the antenna cross sections which have flat(A_0) and V–shaped(A_1) FS. LCMS denotes the Last Closed Magnetic Surface defined by the belt limiters, ATTS represents the Antenna Tile Tangency Surface defined by the tips of antenna protection tiles. δs is the distance LCMS–ATTS and L_{II}^{1} is the parallel connection length within the "private SOL" of the antenna.

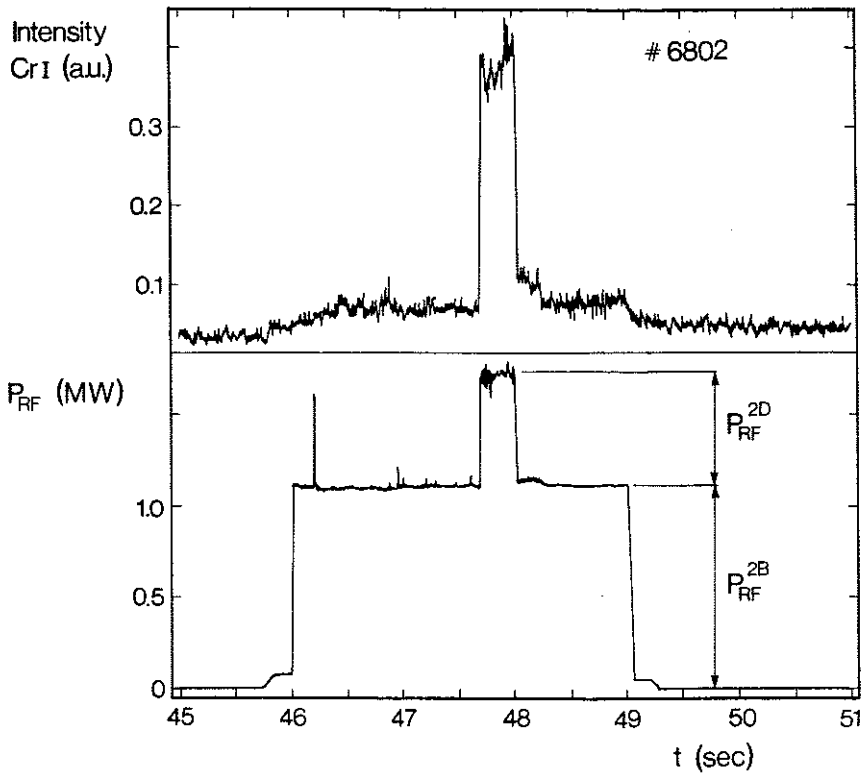

Fig.2. The CrI line intensity which is the measure of the neutral Cr influx monitored at the Cr coated Faraday screen of antenna 2D(type A_0). Corresponding RF powers P_{RF}^{2D} and the P_{RF}^{2B}(adjacent antenna) are also shown.

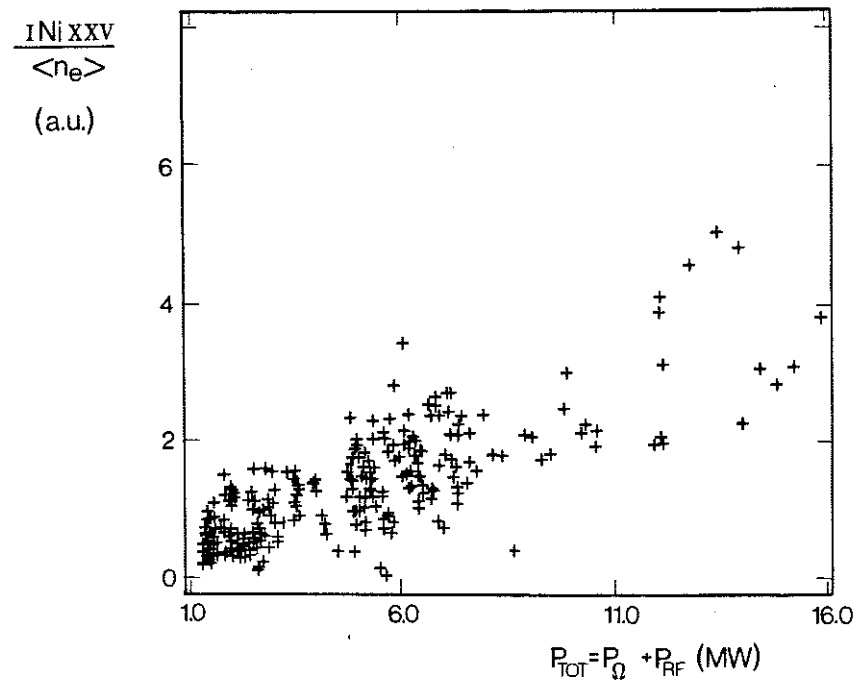

Fig.3. Intensity of NiXXV line normalised to the volume averaged density as a function of the total input of power. INiXXV/$<n_e>$ is a measure of the total amount of NiXXV ions along the spectrometer line of sight.

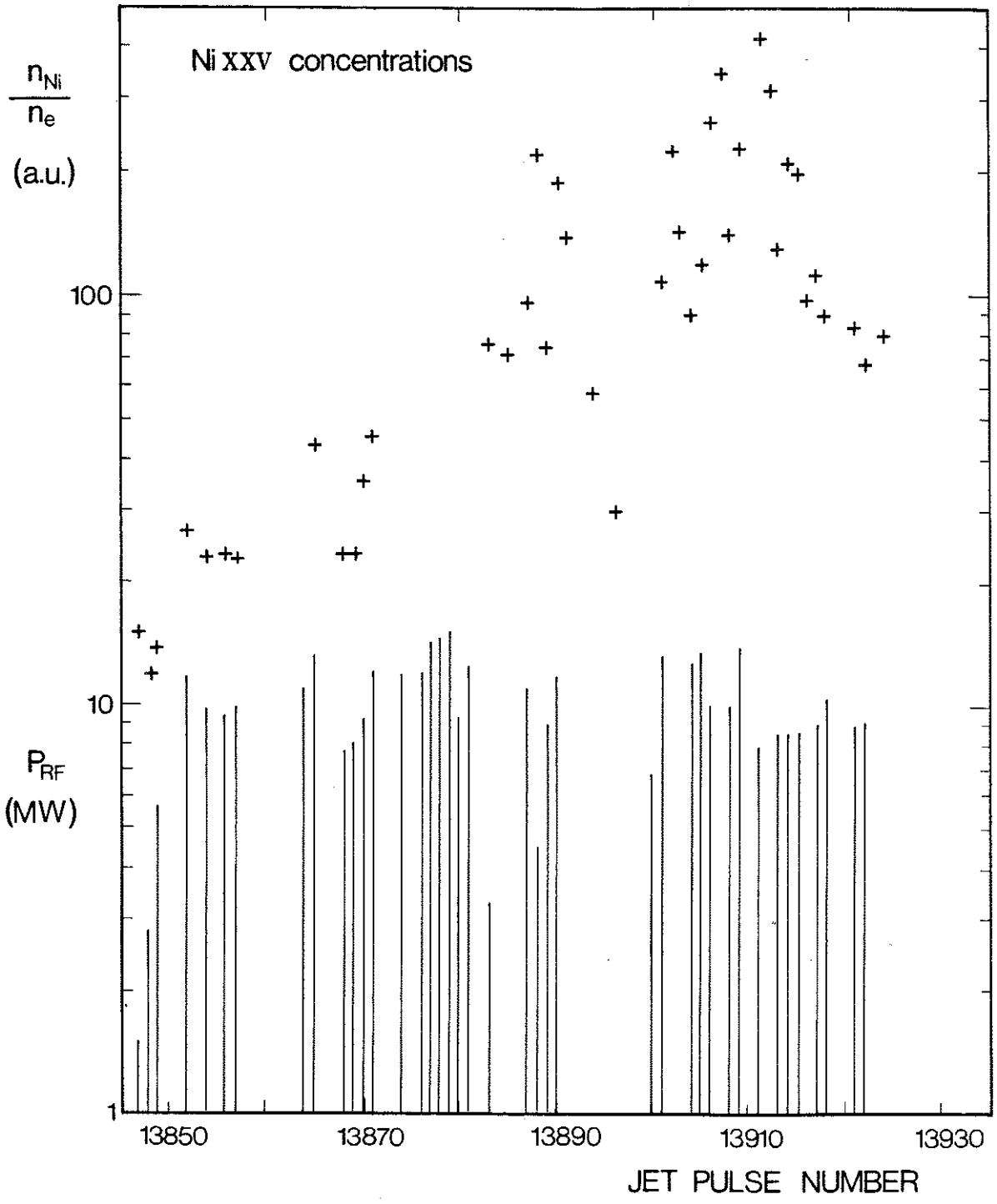

Fig.4. Uncalibrated Ni concentrations measured during the ohmic phase of the discharge, before the application of RF power, as a function of pulse number. The solid lines represent the amount of coupled RF power. The evolution indicates the process of Ni accumulation on belt limiters.

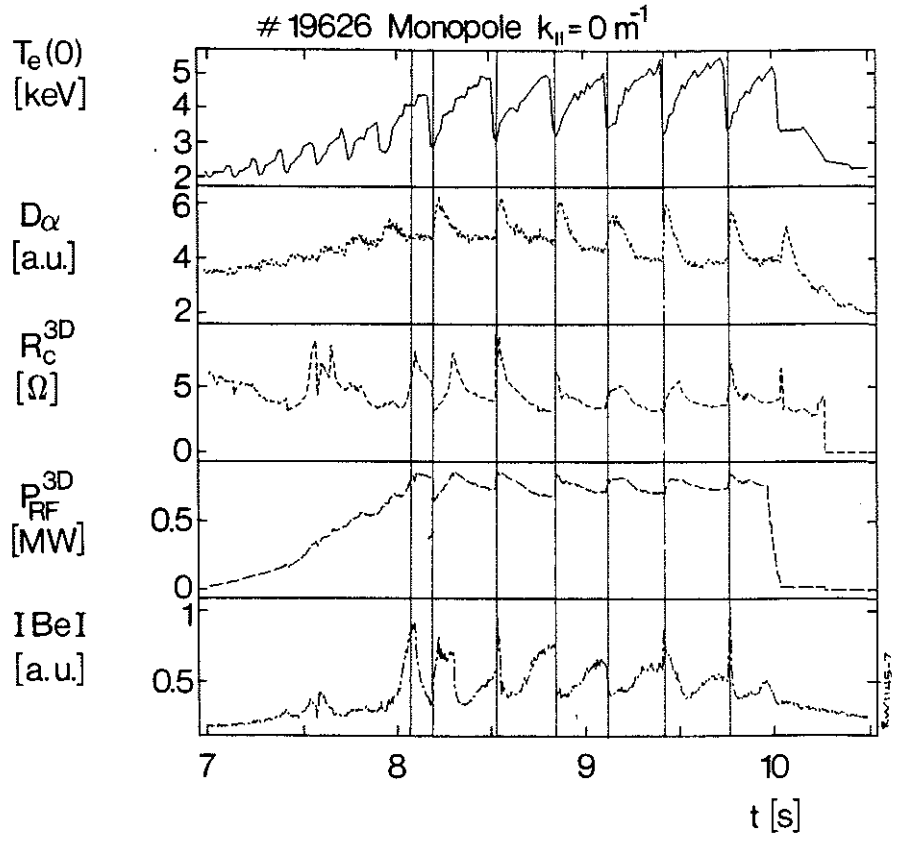

Fig.5a. Evolution of the central electron temperature $T_e(0)$, deuterium recycling on limiter D_α, coupling resistance R_c^{3D} and coupled power P_{RF}^{3D} of antenna 3D and intensity of the BeI line measured along the line of sight interscepting the FS of antenna 3D.

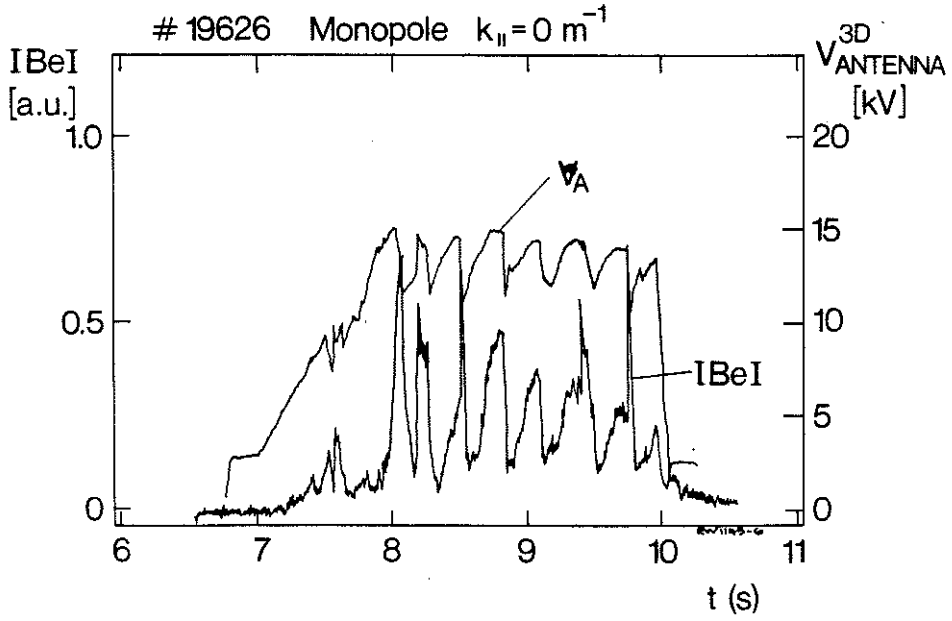

Fig.5b. Correlation of the antenna line voltage V_l(in figure denoted V_A) with the IBeI signal, V_l defined in the text, is calculated from P_{RF}^{3D} and R_C^{3D} for the same discharge as in Fig.5a. IBeI is the same signal as in Fig.5a but plotted with a different scale to illustrate the correlation with V_l.

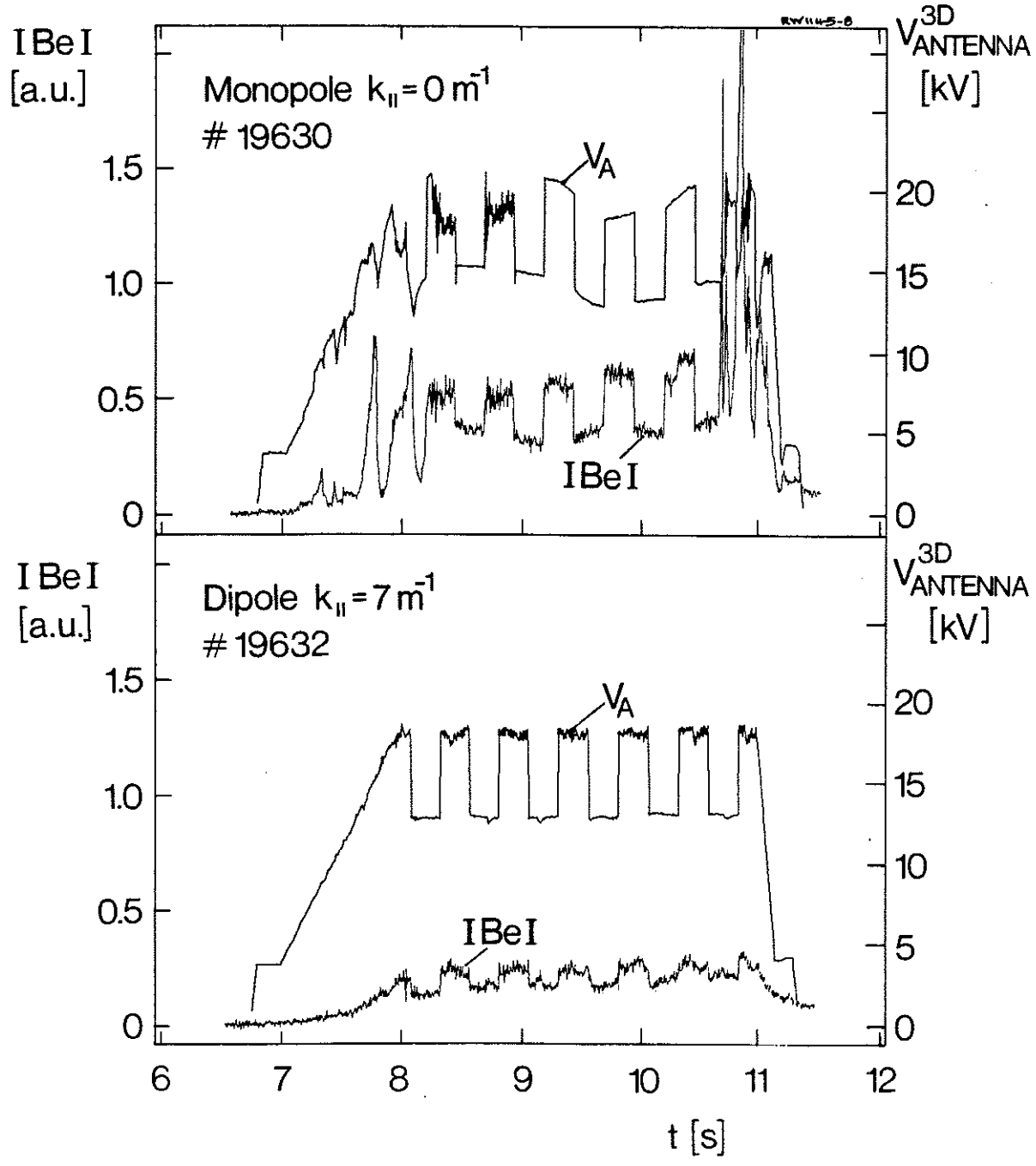

Fig.6. Evolution of antenna line voltage V_I(in figure denoted V_A) and the corresponding IBeI measured at the FS in two similar discharges with monopole and dipole phasing. The discharges were run in the torus with the C–belt limiters. The RF voltage was modulated to check the time scale of the influx response.

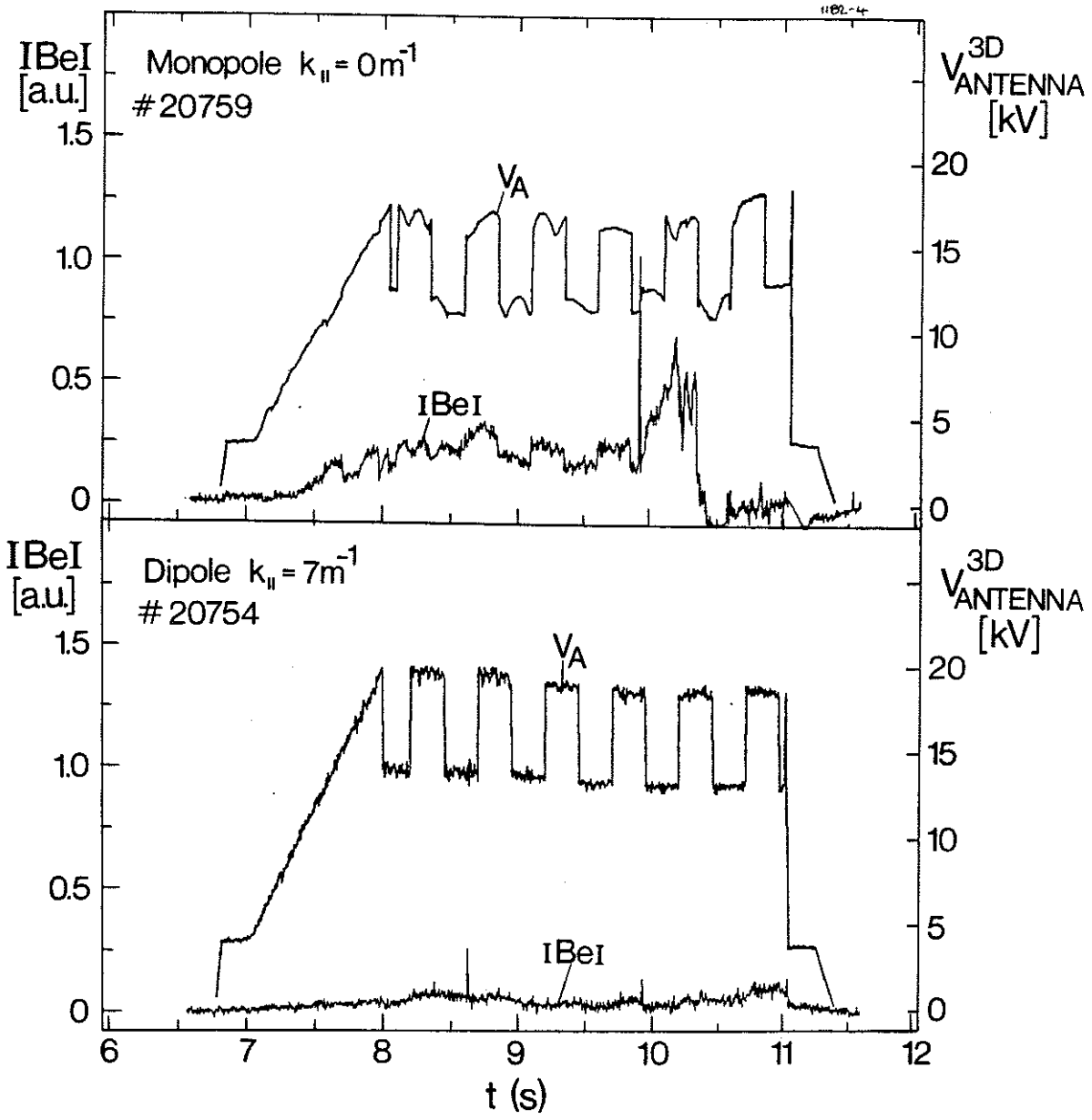

Fig.7. Evolution of antenna line voltage V_l(in figure denoted V_A) and the corresponding IBeI measured at the FS in two similar discharges with monopole and dipole phasing. The discharges were run in the torus with the Be–belt limiters.The RF voltage was modulated to check the time scale of the influx response.

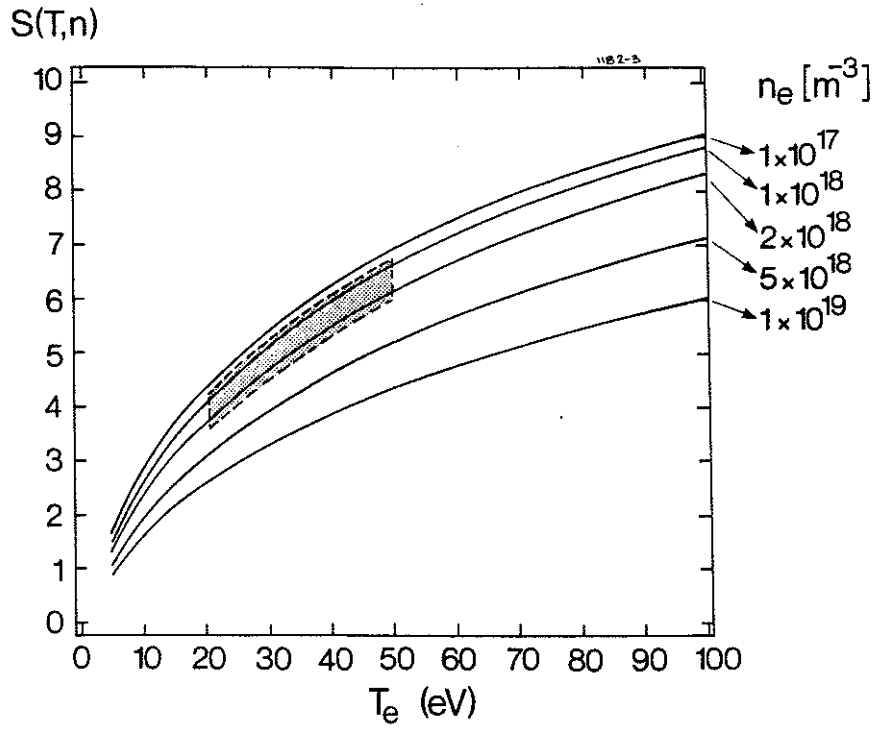

Fig.8. Photon efficiency(number of ionisations per excitation) for the BeI line as a function of temperature and density. The shaded area represents the range of T_e, n_e parameters relevant to the experiments discussed in section 4.2.

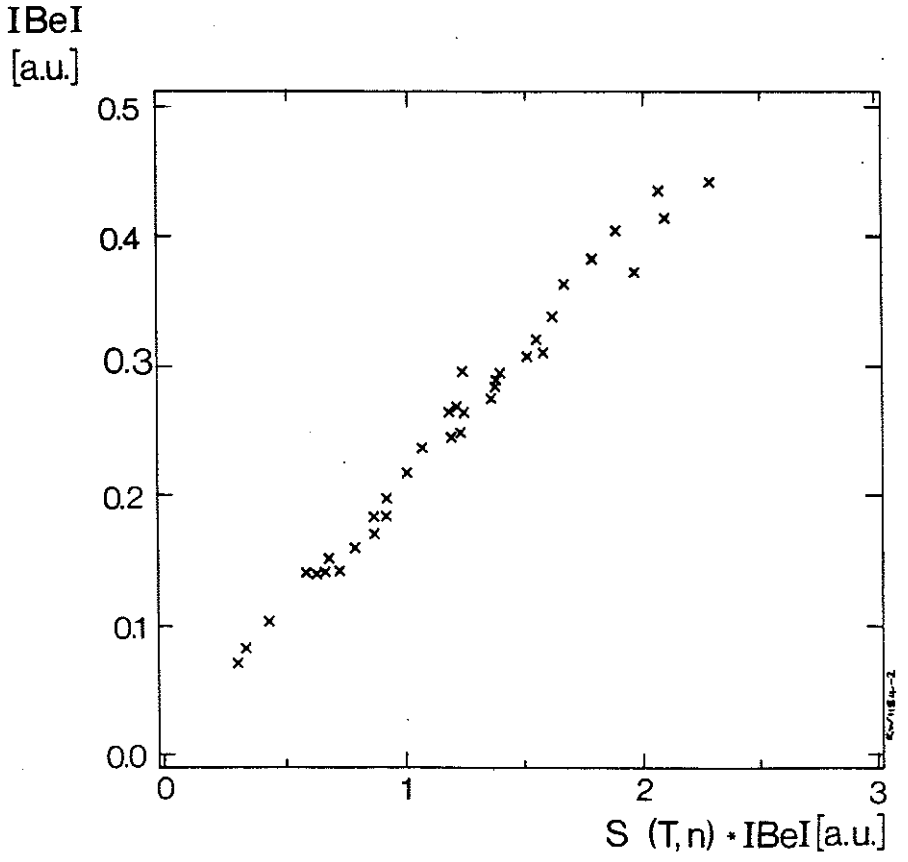

Fig.9. Uncalibrated IBeI plotted against the values corrected for the photon efficiency shown in Fig.8.

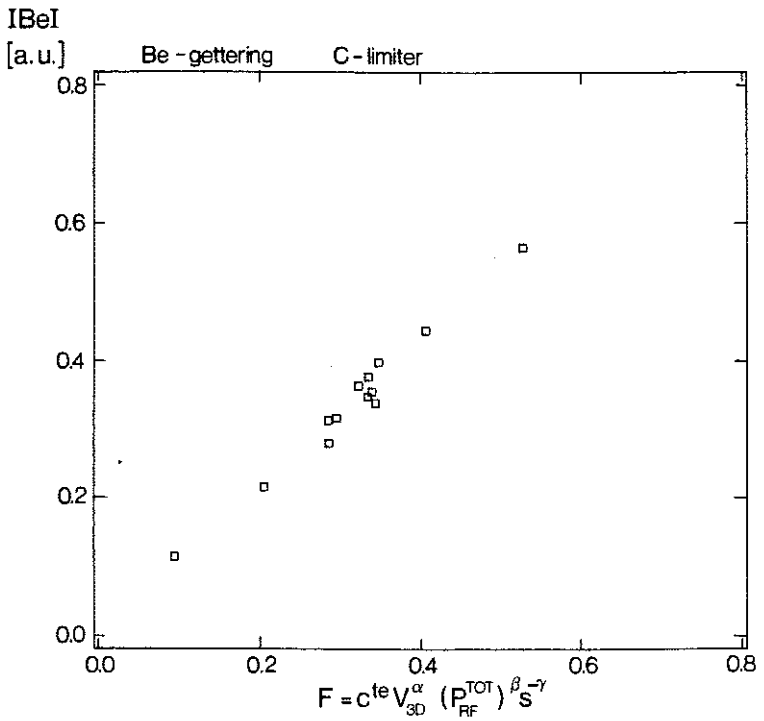

Fig.10. Regression analysis performed on a data set of IBeI monitored at the FS. The data refer to the monopole phasing and C–belt limiter case. Constant $c^{te}=9x10^{-3}$. The error bars of the exponents are quoted in the text. The V_{3D} denotes the antenna line voltage V_l corresponding to the antenna 3D.

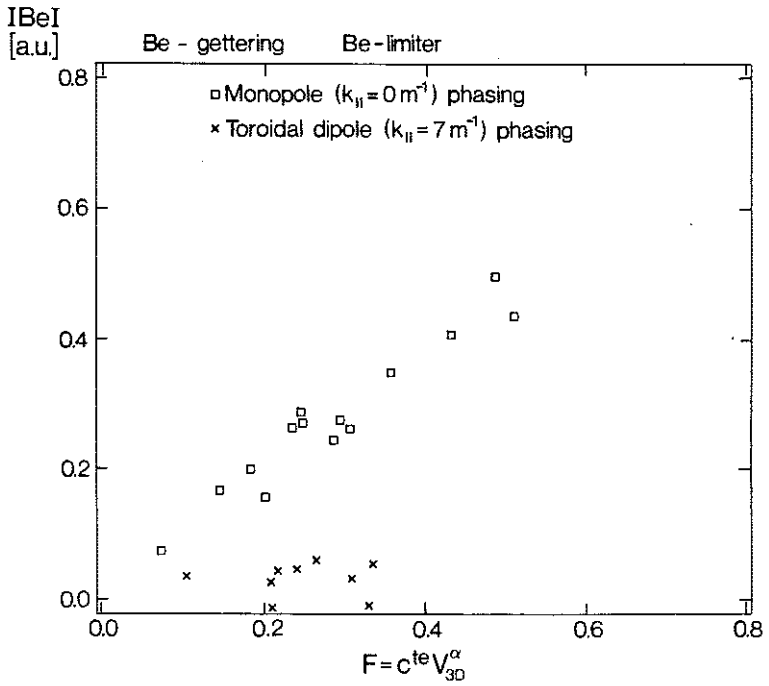

Fig.11. Regression analysis performed on a monopole data set of IBeI monitored at the FS. The dipole points are shown for comparison. All discharges were run in the torus with the Be–belt limiters. Constant $c^{te}=1.05x10^{-3}$. The error bar of the exponent is quoted in the text. The V_{3D} denotes the antenna line voltage V_l corresponding to the antenna 3D.

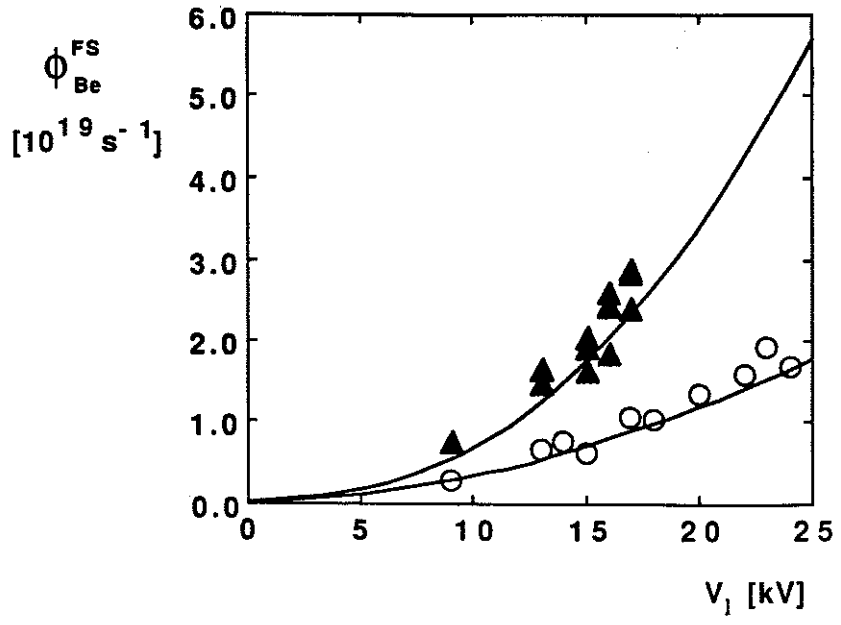

Fig.12. Be influx(measured by IBeI at the FS) versus antenna line voltage V_l for the two cases of C and Be–belt limiters with monopole phasing. The data are normalized to the estimated flux $\phi_{Be}^{FS} = 2 \times 10^{19}$ atoms MW^{-1} s^{-1} and the data for the C limiter case are corrected for the erosion decay(see Sec.4.2 for a discussion). The solid lines represent the theoretical model calculation discussed in Sec. 6.0.

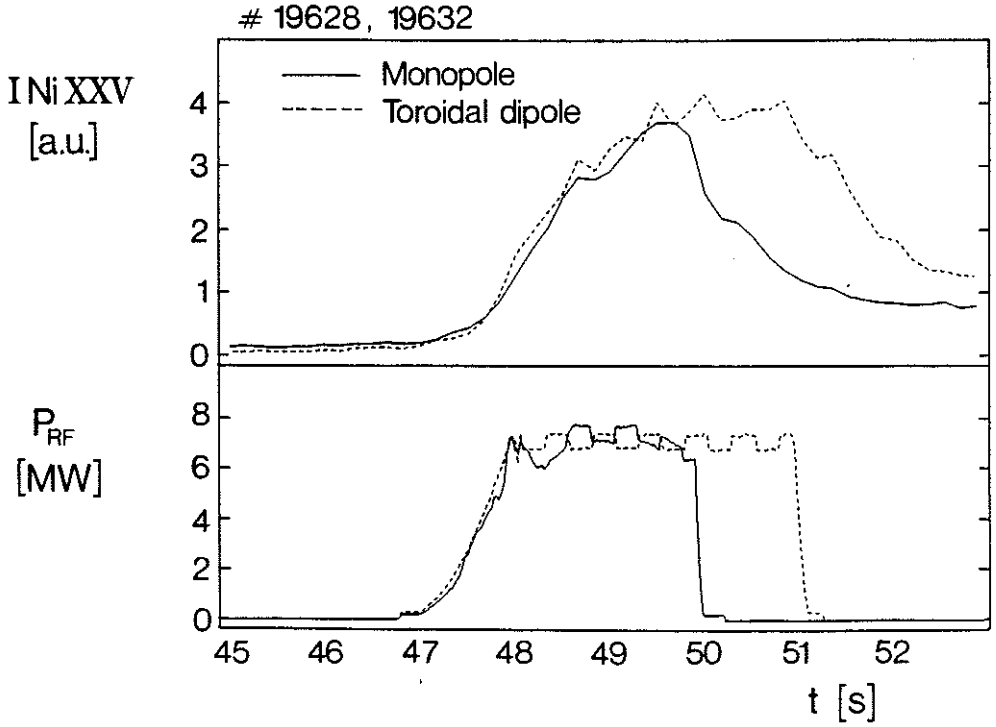

Fig.13. Intensity of NiXXV line monitored by the VUV spectrometer during two discharges with similar plasma densities. The same RF power was launched with different antenna phasing.

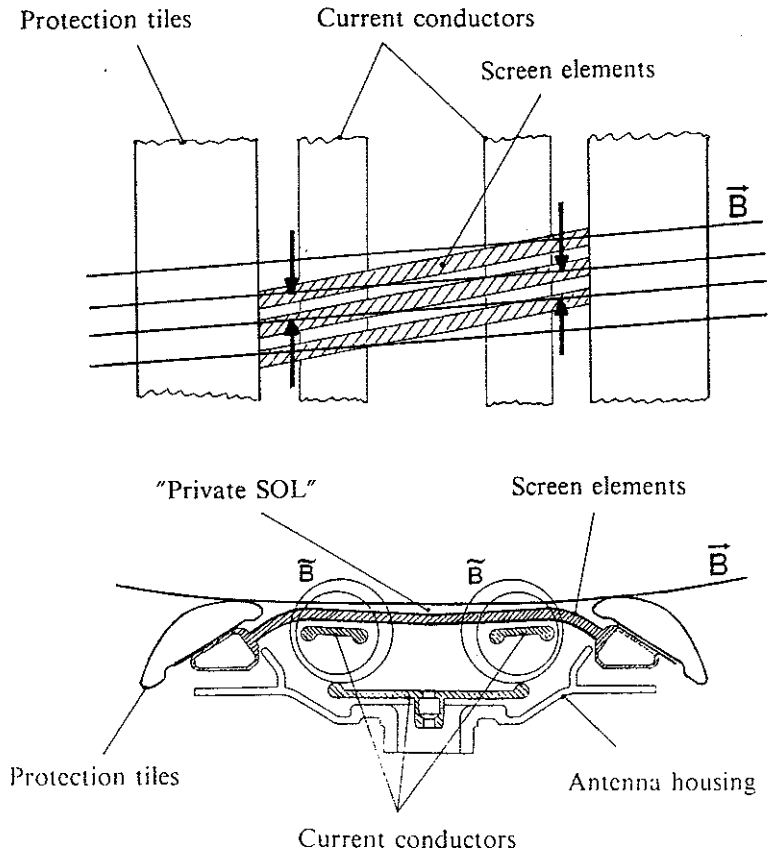

Fig.14. Schematic drawing of the A_1 antenna cross section and the fraction of the FS front view. The closure of the FS front face electric circuits and the points of the enhanced RF sheaths formation are indicated.

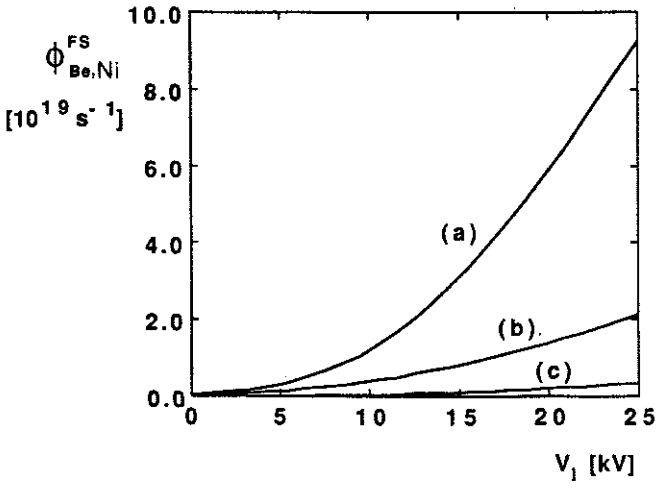

Fig.15. FS impurity influx calculated from the theoretical model versus antenna line voltage V_1 for three cases:(a) C limiter and Ni FS with monopole phasing; (b) Be limiter and Be FS with monopole phasing; (c) Be limiter and Be FS with dipole phasing. The large increase in the ratio of the Ni/Be influx at large voltages is due to Ni self–sputtering.

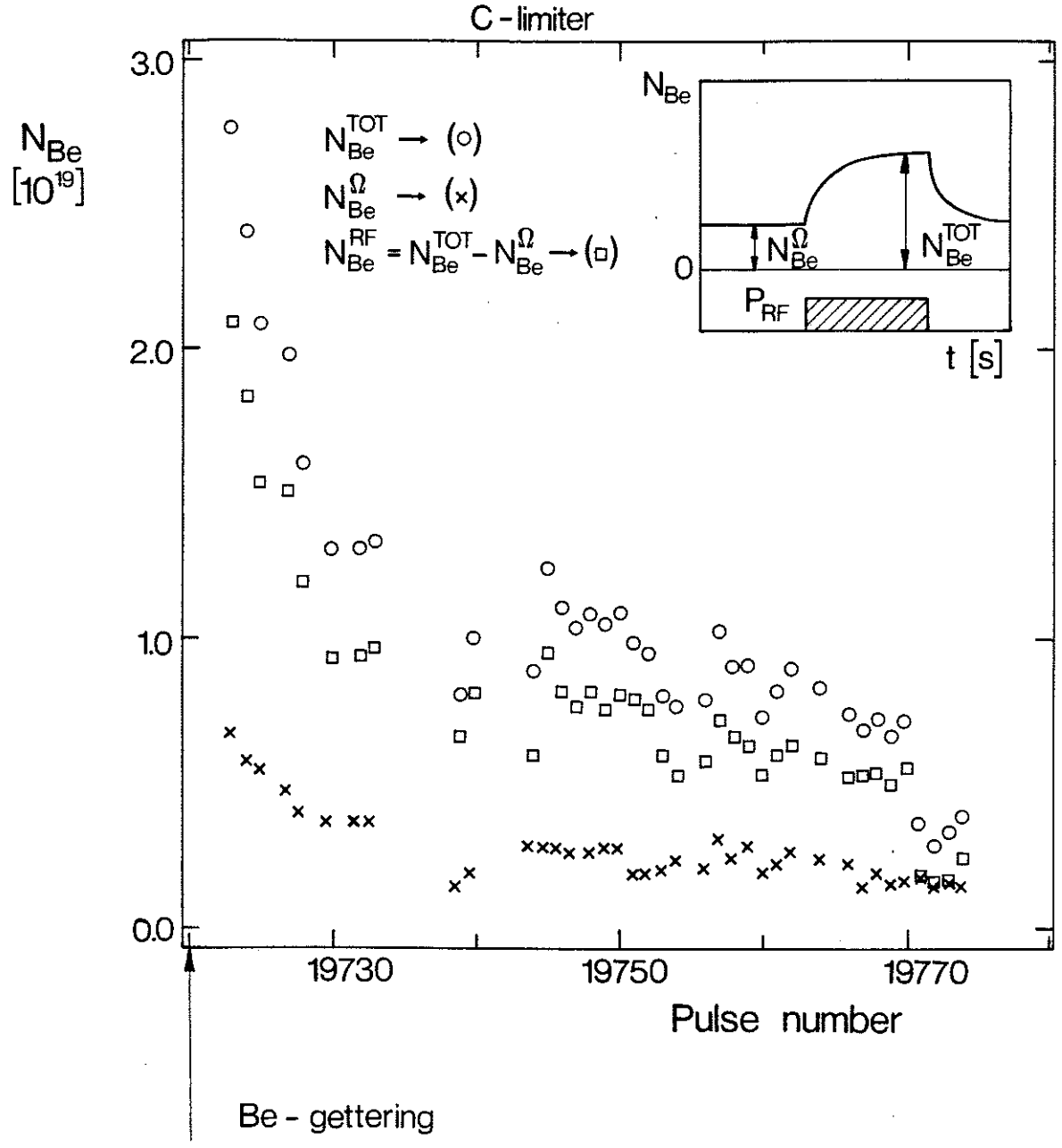

Fig.16. Number of Be ions in the plasma as a function of pulse number after the Be–gettering. The quantities N_{Be}^{TOT} and N_{Be}^{Ω} are defined in the schematic drawing in the inset.

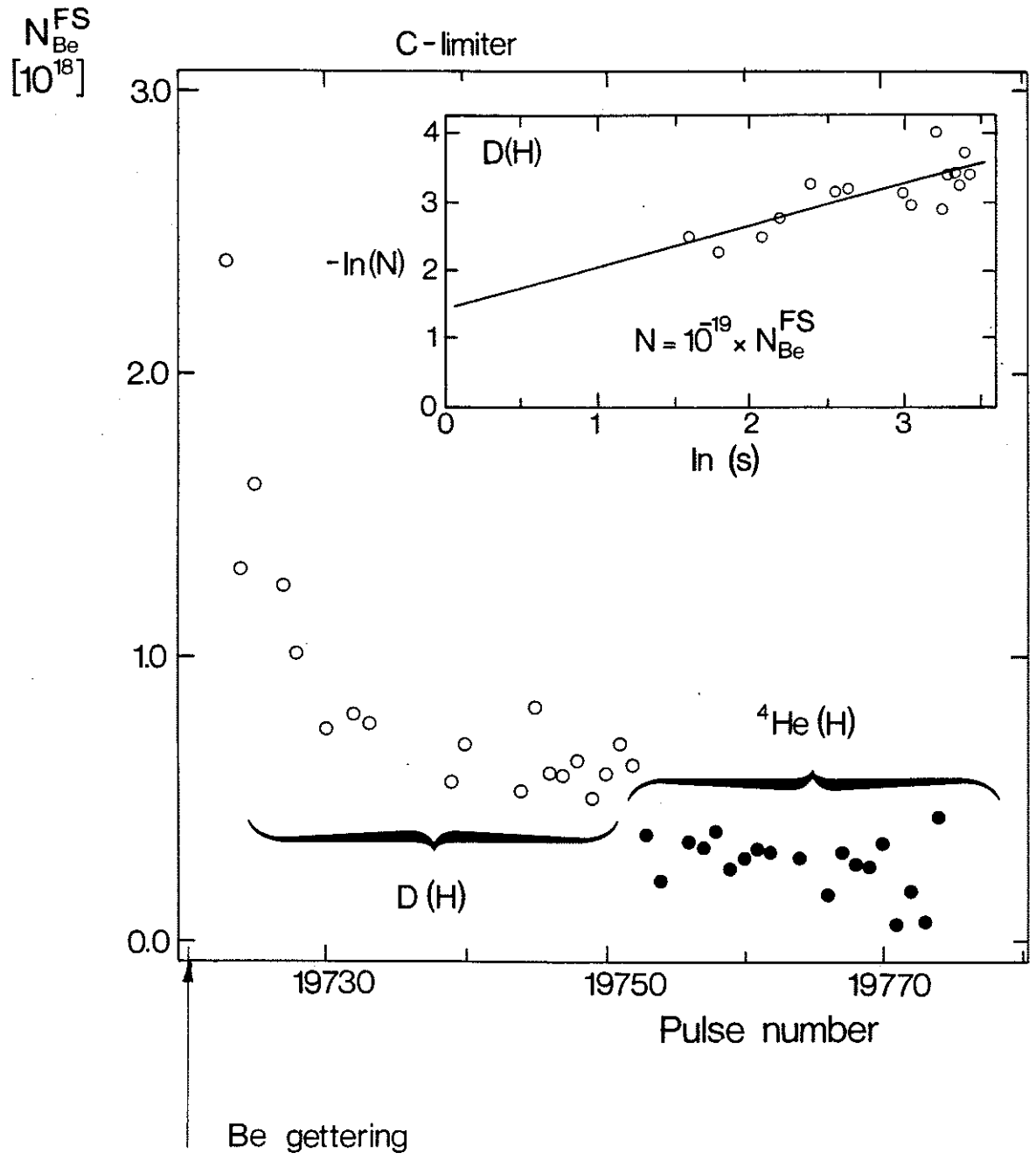

Fig.17. Number of Be ions originating at the FS, normalised to the total RF power, as a function of the pulse number. In the inset the least square fit to the D(H) data is plotted in order to obtain N_o, which is defined $N=N_o s^{-\gamma}$ and $N=10^{-19} \times N_{Be}^{FS}$.

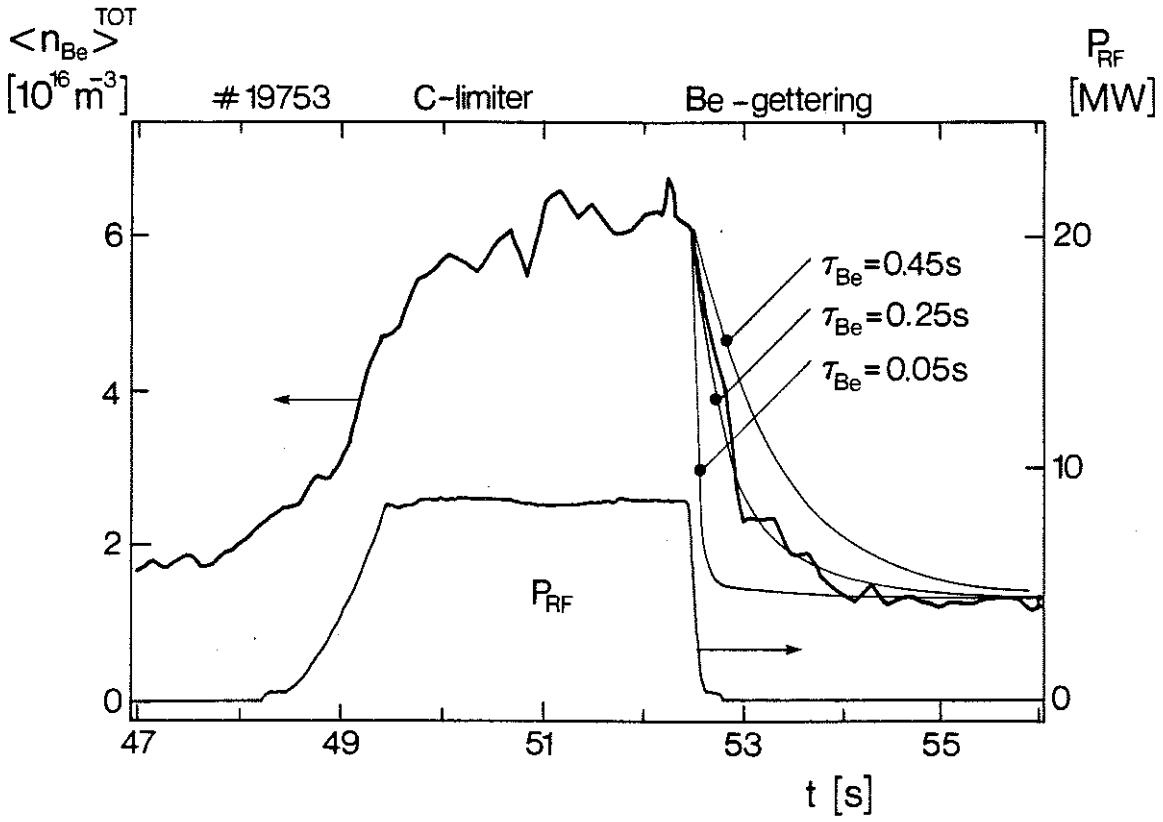

Fig.18. The time evolution of the Be density $\langle n_{Be} \rangle^{TOT}$ as a function of time for a typical RF heated discharge with P_{RF}= 8.3 MW. Here $\langle n_{Be} \rangle^{LIM} \approx \langle n_{Be} \rangle^{RF}/2$ and τ_{INC}= 0.42 s. Three theoretical decays were fitted with τ_{Be}= 0.05, 0.25 and 0.45 s. The best fit corresponds to the confinement time τ_{Be}= 0.2 – 0.25 s. The number of Be ions in the plasma is obtained by multiplying the signal by the plasma volume.

APPENDIX 1.

THE JET TEAM

JET Joint Undertaking, Abingdon, Oxon, OX14 3EA, U.K.

J.M.Adams[1], F.Alladio[4], H.Altmann, R.J.Anderson, G.Appruzzese, W.Bailey, B.Balet, D.V.Bartlett, L.R.Baylor[24], K.Behringer, A.C.Bell, P.Bertoldi, E.Bertolini, V.Bhatnagar, R.J.Bickerton, A.Boileau[3], T.Bonicelli, S.J.Booth, G.Bosia, M.Botman, D.Boyd[31], H.Brelen, H.Brinkschulte, M.Brusati, T.Budd, M.Bures, T.Businaro[4], H.Buttgereit, D.Cacaut, C.Caldwell-Nichols, D.J.Campbell, P.Card, J.Carwardine, G.Celentano, P.Chabert[27], C.D.Challis, A.Cheetham, J.Christiansen, C.Christodoulopoulos, P.Chuilon, R.Claesen, S.Clement[30], J.P.Coad, P.Colestock[6], S.Conroy[13], M.Cooke, S.Cooper, J.G.Cordey, W.Core, S.Corti, A.E.Costley, G.Cottrell, M.Cox[7], P.Cripwell[13], F.Crisanti[4], D.Cross, H.de Blank[16], J.de Haas[16], L.de Kock, E.Deksnis, G.B.Denne, G.Deschamps, G.Devillars, K.J.Dietz, J.Dobbing, S.E.Dorling, P.G.Doyle, D.F.Düchs, H.Duquenoy, A.Edwards, J.Ehrenberg[14], T.Elevant[12], W.Engelhardt, S.K.Erents[7], L.G.Eriksonn[5], M.Evrard[2], H.Falter, D.Flory, M.Forrest[7], C.Froger, K.Fullard, M.Gadeberg[11], A.Galetsas, R.Galvao[8], A.Gibson, R.D.Gill, A.Gondhalekar, C.Gordon, G.Gorini, C.Gormezano, N.A.Gottardi, C.Gowers, B.J.Green, F.S.Griph, M.Gryzinski[26], R.Haange, G.Hammett[6], W.Han[9], C.J.Hancock, P.J.Harbour, N.C.Hawkes[7], P.Haynes[7], T.Hellsten, J.L.Hemmerich, R.Hemsworth, R.F.Herzog, K.Hirsch[14], J.Hoekzema, W.A.Houlberg[24], J.How, M.Huart, A.Hubbard, T.P.Hughes[32], M.Hugon, M.Huguet, J.Jacquinot, O.N.Jarvis, T.C.Jernigan[24], E.Joffrin, E.M.Jones, L.P.D.F.Jones, T.T.C.Jones, J.Källne, A.Kaye, B.E.Keen, M.Keilhacker, G.J.Kelly, A.Khare[15], S.Knowlton, A.Konstantellos, M.Kovanen[21], P.Kupschus, P.Lallia, J.R.Last, L.Lauro-Taroni, M.Laux[33], K.Lawson[7], E.Lazzaro, M.Lennholm, X.Litaudon, P.Lomas, M.Lorentz-Gottardi[2], C.Lowry, G.Magyar, D.Maisonnier, M.Malacarne, V.Marchese, P.Massmann, L.McCarthy[28], G.McCracken[7], P.Mendonca, P.Meriguet, P.Micozzi[4], S.F.Mills, P.Millward, S.L.Milora[24], A.Moissonnier, P.L.Mondino, D.Moreau[17], P.Morgan, H.Morsi[14], G.Murphy, M.F.Nave, M.Newman, L.Nickesson, P.Nielsen, P.Noll, W.Obert, D.O'Brien, J.O'Rourke, M.G.Pacco-Düchs, M.Pain, S.Papastergiou, D.Pasini[20], M.Paume[27], N.Peacock[7], D.Pearson[13], F.Pegoraro, M.Pick, S.Pitcher[7], J.Plancoulaine, J-P.Poffé, F.Porcelli, R.Prentice, T.Raimondi, J.Ramette[17], J.M.Rax[27], C.Raymond, P-H.Rebut, J.Removille, F.Rimini, D.Robinson[7], A.Rolfe, R.T.Ross, L.Rossi, G.Rupprecht[14], R.Rushton, P.Rutter, H.C.Sack, G.Sadler, N.Salmon[13], H.Salzmann[14], A.Santagiustina, D.Schissel[25], P.H.Schild, M.Schmid, G.Schmidt[6], R.L.Shaw, A.Sibley, R.Simonini, J.Sips[16], P.Smeulders, J.Snipes, S.Sommers, L.Sonnerup, K.Sonnenberg, M.Stamp, P.Stangeby[19], D.Start, C.A.Steed, D.Stork, P.E.Stott, T.E.Stringer, D.Stubberfield, T.Sugie[18], D.Summers, H.Summers[20], J.Taboda-Duarte[22], J.Tagle[30], H.Tamnen, A.Tanga, A.Taroni, C.Tebaldi[23], A.Tesini, P.R.Thomas, E.Thompson, K.Thomsen[11], P.Trevalion, M.Tschudin, B.Tubbing, K.Uchino[29], E.Usselmann, H.van der Beken, M.von Hellermann, T.Wade, C.Walker, B.A.Wallander, M.Walravens, K.Walter, D.Ward, M.L.Watkins, J.Wesson, D.H.Wheeler, J.Wilks, U.Willen[12], D.Wilson, T.Winkel, C.Woodward, M.Wykes, I.D.Young, L.Zannelli, M.Zarnstorff[6], D.Zasche[14], J.W.Zwart.

PERMANENT ADDRESS

1. UKAEA, Harwell, Oxon. UK.
2. EUR-EB Association, LPP-ERM/KMS, B-1040 Brussels, Belgium.
3. Institute National des Récherches Scientifique, Quebec, Canada.
4. ENEA-CENTRO Di Frascati, I-00044 Frascati, Roma, Italy.
5. Chalmers University of Technology, Göteborg, Sweden.
6. Princeton Plasma Physics Laboratory, New Jersey, USA.
7. UKAEA Culham Laboratory, Abingdon, Oxon. UK.
8. Plasma Physics Laboratory, Space Research Institute, Sao José dos Campos, Brazil.
9. Institute of Mathematics, University of Oxford, UK.
10. CRPP/EPFL, 21 Avenue des Bains, CH-1007 Lausanne, Switzerland.
11. Risø National Laboratory, DK-4000 Roskilde, Denmark.
12. Swedish Energy Research Commission, S-10072 Stockholm, Sweden.
13. Imperial College of Science and Technology, University of London, UK.
14. Max Planck Institut für Plasmaphysik, D-8046 Garching bei München, FRG.
15. Institute for Plasma Research, Gandhinagar Bhat Gujat, India.
16. FOM Instituut voor Plasmafysica, 3430 Be Nieuwegein, The Netherlands.
17. Commissiariat à L'Energie Atomique, F-92260 Fontenay-aux-Roses, France.
18. JAERI, Tokai Research Establishment, Tokai-Mura, Naka-Gun, Japan.
19. Institute for Aerospace Studies, University of Toronto, Downsview, Ontario, Canada.
20. University of Strathclyde, Glasgow, G4 ONG, U.K.
21. Nuclear Engineering Laboratory, Lapeenranta University, Finland.
22. JNICT, Lisboa, Portugal.
23. Department of Mathematics, Univeristy of Bologna, Italy.
24. Oak Ridge National Laboratory, Oak Ridge, Tenn., USA.
25. G.A. Technologies, San Diego, California, USA.
26. Institute for Nuclear Studies, Swierk, Poland.
27. Commissiariat à l'Energie Atomique, Cadarache, France.
28. School of Physical Sciences, Flinders University of South Australia, South Australia SO42.
29. Kyushi University, Kasagu Fukuoka, Japan.
30. Centro de Investigaciones Energeticas Medioambientales y Techalogicas, Spain.
31. University of Maryland, College Park, Maryland, USA.
32. University of Essex, Colchester, UK.
33. Akademie de Wissenschaften, Berlin, DDR.

CR 88.49.1A